

Phenomenological Comparison of the Dark Phases of the Next-to-Two-Higgs-Doublet Model

Isabell Engeln

Master Thesis

At the Department of Physics
Institut für Teilchenphysik (ITP)

Reviewer: Prof. Dr. Margarete Mühlleitner
Second reviewer: Prof. Dr. Thomas Schwetz-Mangold

Duration: March 20, 2017 – March 7, 2018

Statement of Authorship

I declare that I have developed and written the enclosed thesis completely by myself, and have not used sources or means without declaration in the text. I further confirm that I have respected statute of good scientific practice of the KIT in its current version.

Karlsruhe, March 7, 2018

.....
(Isabell Engeln)

Accepted as Master thesis.

Karlsruhe, March 7, 2018

.....
(Prof. Dr. Margarete Mühlleitner)

Contents

1. Introduction	1
2. The Next-to-Two-Higgs-Doublet Model	3
2.1. The Scalar Lagrangian	3
2.2. The Yukawa Lagrangian	5
3. The Dark Phases of the Next-to-Two-Higgs-Doublet Model	7
3.1. The Inert Doublet Phase	7
3.1.1. Diagonalisation of the Scalar Sector	7
3.1.2. Parametrisation of the Potential in Terms of Physical Parameters . .	8
3.1.3. Higgs Couplings to SM Particles	8
3.1.3.1. The Visible Sector	9
3.1.3.2. The Dark Sector	9
3.2. The Dark Singlet Phase	9
3.2.1. Diagonalisation of the Scalar Sector	9
3.2.2. Parametrisation of the Potential in Terms of Physical Parameters . .	10
3.2.3. Higgs Couplings	10
4. Theoretical and Experimental Constraints	11
4.1. Vacuum Stability	11
4.1.1. Conditions for the Potential to be Bounded from Below	11
4.1.2. Vacuum Decay and Global Minimum Conditions	12
4.2. Tree-Level Perturbative Unitarity	13
4.3. Signal Strengths of the h_{125}	15
4.4. Electroweak Precision Measurements	15
4.5. B-Physics Measurements	15
4.6. Dark Matter Relic Density and Direct Detection	16
5. Scans of the Parameter Space	19
5.1. Description of the Used Tools	19
5.1.1. ScannerS	19
5.1.2. MicrOMEGAs	20
5.2. The Samples of Parameter Points	20
5.2.1. Basics of Sample Generation	20
5.2.2. Scan Ranges	20
6. Phenomenological Results	23
6.1. Properties of the h_{125}	23
6.1.1. Couplings to SM Particles	24
6.1.2. Signal Strengths at Collider Experiments	25
6.2. Mass Distributions of the Additional Scalars	28
6.2.1. Mass Splittings of the Dark Scalars in the Inert Doublet Phase . . .	29
6.2.2. Mass Ranges of the Visible Scalars in the Dark Singlet Phase	30

6.3. Distinguishing the Dark Phases Through the Properties of the Additional Higgs Bosons	30
6.4. The Impact of Dark Matter Direct Detection Constraints	34
6.4.1. Dark Matter Nucleon Cross Sections	34
6.4.2. The Impact on the Visible Sector	35
6.4.3. The Impact on the Dark Sector	35
7. Conclusion	39
A. Appendix: Inert Doublet Phase	41
A.1. Explicit Parameter Transformations	41
A.2. Triple-Higgs Couplings	42
B. Appendix: Dark Singlet Phase	43
B.1. Explicit Parameter Transformations	43
B.2. Triple-Higgs Couplings	44
C. Global Minimum Conditions for the \mathbb{Z}_2-Conserving Potential	45
C.1. 2HDM-Like Stationary Points	45
C.1.1. Case I	45
C.1.2. Case III	46
C.1.3. Case IV	46
C.1.4. Case V	47
C.2. Stationary Points With a Non-Zero Singlet Vacuum Expectation Value . . .	47
C.2.1. Case sI	47
C.2.2. Case sIII	47
C.2.3. Case sIV	48
C.2.4. Case sV	48
C.2.5. Case s	49
C.3. Special Cases	49
C.4. Summary	50
Acknowledgements	51
Glossary	53
Bibliography	55

1. Introduction

Since the discovery of the Higgs Boson in 2012 [1, 2] has added the last missing part to the Standard Model (SM) of Particle Physics, the search for dark matter (DM) has become one of the most pressing puzzles. There are many evidences of DM, ranging from gravitational effects on astrophysical scales and the large-scale structure of the Universe to the measurement of baryon acoustic oscillations in the cosmic microwave background radiation [3], which revealed that the relic abundance of DM in the Universe is about 26% [4–6]. But only few is known on the nature of DM.

The SM contains three candidates for DM: the electron, muon and tau neutrinos. However, SM neutrinos as the main component of DM are in contradiction with cosmological observations of structure formation [7]. A popular candidate for DM that can reproduce structure formation as well as the observed relic abundance is the so-called weakly interacting massive particle (WIMP) with a mass of $\mathcal{O}(100)$ GeV and an interaction cross section with SM particles comparable to that of the weak force.

In order to obtain a WIMP as DM candidate, we need to extend the SM. Since the SM is in excellent agreement with experimental measurements, physics beyond the SM (BSM) is strongly constrained in order to match the observations within experimental uncertainties. One of the most restrictive constraints on BSM models is the ρ parameter, which indicates the relative strength of neutral and charged-current interactions in processes with four fermions and zero momentum transfer [8]. In the SM, the ρ parameter equals to one at tree level. When adding only $SU(2)$ doublets or singlets the ρ parameter remains unity at tree-level. Thus, one of the simplest WIMP models is the scalar singlet DM scenario [9–11] which extends the SM by a real singlet field. The additional singlet is uncharged under the SM gauge groups and stabilised by a \mathbb{Z}_2 symmetry. Therefore, it forms a dark sector providing one neutral CP-even DM candidate. This model has already been extensively studied, see e.g. [12–15]. Another well-studied model for WIMP DM is the so-called inert doublet model (IDM) [16–19], an extension of the SM by a dark Higgs doublet. Similar to the dark singlet extension, the additional doublet in the IDM is protected by a \mathbb{Z}_2 symmetry and forms a dark sector containing one charged and two neutral fields, one CP-even and one CP-odd.

In the Next-to-Two-Higgs-Doublet Model (N2HDM) [20–23], which extends the scalar sector of the SM by one doublet and one real singlet, both of these approaches can be realised as different phases of electroweak symmetry breaking (EWSB) based on one common scalar sector. This model introduces two \mathbb{Z}_2 symmetries, one of which can stabilise the additional

doublet, while the other stabilises the additional singlet. In the absence of soft breaking each of these \mathbb{Z}_2 symmetries can give rise to a dark sector if it is not spontaneously broken by EWSB.

In this work, we compare the N2HDM phases with singlet [21] and doublet DM. We call the phase with singlet DM the dark singlet phase (DSP), which corresponds to a Two-Higgs-Doublet Model (2HDM) [24–26] with a Higgs portal to the dark sector. In our analysis, we focus on the case with couplings to fermions as in a type I 2HDM. In contrast to usual 2HDM studies, we further require the spontaneously broken \mathbb{Z}_2 symmetry to not also be softly broken [27]. The inert doublet phase (IDP) denotes the doublet DM phase as in the IDM. However, the additional scalar singlet can mix with the 125 GeV state and enriches the visible phenomenology by one additional CP-even Higgs boson. In order to study both phases, we implement each phase as a model class in the `ScannerS` framework [28] and perform an extensive scan in the parameter space.

This work is structured as follows. In Chapter 2, we begin with an introduction to the N2HDM. In Chapter 3, we discuss the IDP and DSP in detail including the diagonalisation of the scalar sector and the effective couplings to SM particles for each phase. Chapter 4 is dedicated to the constraints applied on the parameters of each phase or dependent quantities in order to ensure that a generated parameter point agrees with theoretical requirements and experimental measurements. The tools used to generate the samples as well as the parameter scans performed in the two N2HDM phases are described in Chapter 5. In Chapter 6, we finally present the phenomenological analysis regarding the predictions of the properties of the 125 GeV Higgs boson and the ways to distinguish between the IDP and DSP provided that a second Higgs boson is observed. Furthermore, we study the impact of recent exclusion bounds from DM direct detection on the visible and dark sector of each model. Our conclusion is presented in Chapter 7.

2. The Next-to-Two-Higgs-Doublet Model

The N2HDM [20–23] is an extension of the SM, which consists of one additional complex $SU(2)_L$ doublet with hypercharge +1 and one real, hypercharge zero $SU(2)_L$ singlet. In the following, we summarise the implications of this extension for the scalar Lagrangian $\mathcal{L}_{\text{Scalar}}$ (Section 2.1) and the Yukawa Lagrangian $\mathcal{L}_{\text{Yukawa}}$ (Section 2.2).

2.1. The Scalar Lagrangian

The scalar Lagrangian describes the Higgs-Higgs and Higgs-gauge boson interactions and reads

$$\mathcal{L}_{\text{scalar}} = (D_\mu \Phi_i)^\dagger (D^\mu \Phi_i) + (\partial_\mu \Phi_S)(\partial^\mu \Phi_S) - V_{\text{scalar}} \quad (2.1)$$

with the doublets Φ_i ($i \in \{1, 2\}$) and the singlet Φ_S . The electroweak covariant derivative is given by

$$D_\mu = \partial_\mu + ig \frac{\sigma^a}{2} W_\mu^a + ig' \frac{Y}{2} B_\mu, \quad (2.2)$$

where W_μ^a ($a \in \{1, 2, 3\}$) and B_μ are the $SU(2)_L$ and $U(1)_Y$ gauge fields with the corresponding gauge couplings g and g' , respectively. The Pauli matrices σ^a and the hypercharge Y are, combined with the factor of 1/2, the generators of the respective groups. The most general scalar potential of the N2HDM is constructed from all possible combinations of the fields Φ_1, Φ_2, Φ_S in such a way that the potential remains renormalisable. In this work, we only consider the CP-conserving version of the model and additionally impose two \mathbb{Z}_2 symmetries, which are described below. The resulting scalar potential reads

$$\begin{aligned} V_{\text{Scalar}} = & m_{11}^2 \Phi_1^\dagger \Phi_1 + m_{22}^2 \Phi_2^\dagger \Phi_2 - m_{12}^2 (\Phi_1^\dagger \Phi_2 + \text{h.c.}) + \frac{\lambda_1}{2} (\Phi_1^\dagger \Phi_1)^2 + \frac{\lambda_2}{2} (\Phi_2^\dagger \Phi_2)^2 \\ & + \lambda_3 \Phi_1^\dagger \Phi_1 \Phi_2^\dagger \Phi_2 + \lambda_4 \Phi_1^\dagger \Phi_2 \Phi_2^\dagger \Phi_1 + \frac{\lambda_5}{2} \left((\Phi_1^\dagger \Phi_2)^2 + \text{h.c.} \right) \\ & + \frac{1}{2} m_s^2 \Phi_S^2 + \frac{\lambda_6}{8} \Phi_S^4 + \frac{\lambda_7}{2} \Phi_1^\dagger \Phi_1 \Phi_S^2 + \frac{\lambda_8}{2} \Phi_2^\dagger \Phi_2 \Phi_S^2, \end{aligned} \quad (2.3)$$

containing eight real, dimensionless and four real mass parameters, resulting in a total of twelve real parameters. The first \mathbb{Z}_2 symmetry we imposed,

$$\mathbb{Z}_2^{(1)} : \quad \Phi_1 \rightarrow -\Phi_1, \quad \Phi_2 \rightarrow \Phi_2, \quad \Phi_S \rightarrow \Phi_S, \quad (2.4)$$

is the generalisation of the usual \mathbb{Z}_2 symmetry of the 2HDM [24–26] to the N2HDM. This symmetry is softly broken for non-zero m_{12}^2 . The second \mathbb{Z}_2 symmetry,

$$\mathbb{Z}_2^{(2)} : \quad \Phi_1 \rightarrow \Phi_1, \quad \Phi_2 \rightarrow \Phi_2, \quad \Phi_S \rightarrow -\Phi_S, \quad (2.5)$$

is not explicitly broken. If the \mathbb{Z}_2 symmetries are not spontaneously broken, each of them can give rise to one or more DM candidates after EWSB.

The field configuration after EWSB can be parametrised in terms of the charged complex fields ϕ_i^+ ($i \in \{1, 2\}$), the neutral CP-even fields ρ_I ($I \in \{1, 2, s\}$) and the neutral CP-odd fields η_i as follows

$$\Phi_1 = \begin{pmatrix} \phi_1^+ \\ \frac{1}{\sqrt{2}}(v_1 + \rho_1 + i\eta_1) \end{pmatrix}, \quad \Phi_2 = \begin{pmatrix} \phi_2^+ \\ \frac{1}{\sqrt{2}}(v_2 + \rho_2 + i\eta_2) \end{pmatrix}, \quad \Phi_S = v_s + \rho_s. \quad (2.6)$$

Requiring the vacuum expectation values (VEVs)

$$\langle \Phi_i \rangle = \begin{pmatrix} 0 \\ \frac{v_i}{\sqrt{2}} \end{pmatrix} \quad \text{and} \quad \langle \Phi_S \rangle = v_s, \quad (2.7)$$

which break the $SU(2)_L \times U(1)_Y$ down to $U(1)_{EM}$, to be stationary points of the potential leads to three stationary conditions

$$\left\langle \frac{dV}{dv_1} \right\rangle = 0 \Rightarrow v_2 m_{12}^2 - v_1 m_{11}^2 = \frac{1}{2} v_1 (v_1^2 \lambda_1 + v_2^2 (\lambda_3 + \lambda_4 + \lambda_5) + v_s^2 \lambda_7), \quad (2.8a)$$

$$\left\langle \frac{dV}{dv_2} \right\rangle = 0 \Rightarrow v_1 m_{12}^2 - v_2 m_{22}^2 = \frac{1}{2} v_2 (v_1^2 (\lambda_3 + \lambda_4 + \lambda_5) + v_2^2 \lambda_2 + v_s^2 \lambda_8), \quad (2.8b)$$

$$\left\langle \frac{dV}{dv_s} \right\rangle = 0 \Rightarrow -v_s m_s^2 = \frac{1}{2} v_s (v_1^2 \lambda_7 + v_2^2 \lambda_8 + v_s^2 \lambda_6). \quad (2.8c)$$

These will be used to trade the parameters m_{11}^2 , m_{22}^2 and m_s^2 for the VEVs v_1, v_2 and v_s . Considering the CP and charge conserving possible VEV configurations, we distinguish four cases:

The Broken Phase in which both doublets and the singlet acquire non-zero VEVs and, therefore, both \mathbb{Z}_2 symmetries are spontaneously broken by EWSB. This case has been studied in [23].

The Inert Doublet Phase in which only one of the doublets (either Φ_1 or Φ_2) and the singlet acquire non-vanishing VEVs. This phase is the N2HDM equivalent to the Inert Doublet Model of the 2HDM [16–19]. From the Equations (2.8a) and (2.8b) follows that

$$(v_1 = 0 \Leftrightarrow v_2 = 0) \vee m_{12}^2 = 0. \quad (2.9)$$

Therefore, this case is only possible if $\mathbb{Z}_2^{(1)}$ (2.4) is exactly preserved by choosing $m_{12}^2 = 0$. In this phase, DM candidates arise from the inert doublet. This case is discussed in Section 3.1.

The Dark Singlet Phase in which both doublets but not the singlet acquire VEVs. Here, $\mathbb{Z}_2^{(2)}$ (2.5) is unbroken and leads to a DM candidate originating from the singlet. This phase is essentially a 2HDM plus a dark real singlet [9–11] and will be discussed further in Section 3.2.

The SM-Like Phase in which neither the singlet nor the additional doublet acquires a VEV. Similar to the IDP, this case is only possible if the $\mathbb{Z}_2^{(1)}$ soft-breaking term vanishes. Both \mathbb{Z}_2 symmetries remain unbroken and only one doublet couples to SM particles while the other doublet and the singlet form two dark sectors. Since this phase does not provide much interesting collider phenomenology, it is not further discussed in this work.

Depending on the phase, the fields with the same quantum numbers mix with each other. In order to diagonalise the mass matrices of the three neutral CP-even, the two neutral CP-odd and the two charged scalar fields

$$\mathcal{M}_{ij}^\rho = \frac{\partial^2 V_{\text{Scalar}}}{\partial \rho_i \partial \rho_j}, \quad \mathcal{M}_{lm}^\eta = \frac{\partial^2 V_{\text{Scalar}}}{\partial \eta_l \partial \eta_m}, \quad \mathcal{M}_{lm}^\pm = \frac{\partial^2 V_{\text{Scalar}}}{\partial \phi_l^\pm \partial \phi_m^\pm}, \quad (2.10)$$

where $i, j \in \{1, 2, s\}$ and $l, m \in \{1, 2\}$, we introduce two mixing matrices \mathcal{R} and \mathcal{U} that rotate from the basis of gauge eigenstates into the basis of mass eigenstates as follows

$$\begin{pmatrix} H_1 \\ H_2 \\ H_3 \end{pmatrix} = \mathcal{R} \begin{pmatrix} \rho_1 \\ \rho_2 \\ \rho_s \end{pmatrix}, \quad \begin{pmatrix} G^0 \\ A \end{pmatrix} = \mathcal{U} \begin{pmatrix} \eta_1 \\ \eta_2 \end{pmatrix}, \quad \begin{pmatrix} G^\pm \\ H^\pm \end{pmatrix} = \mathcal{U} \begin{pmatrix} \phi_1^\pm \\ \phi_2^\pm \end{pmatrix}. \quad (2.11)$$

The H_i ($i \in \{1, 2, 3\}$) are the neutral CP-even mass eigenstates. A is the neutral CP-odd and H^\pm are the charged mass eigenstates. G^0 and G^\pm are the neutral and charged would-be Goldstone bosons that provide the gauge bosons with their longitudinal component.

2.2. The Yukawa Lagrangian

The interactions of fermions and Higgs fields are described in the Yukawa Lagrangian, which reads in the N2HDM, as in the 2HDM [29],

$$\mathcal{L}_{\text{Yukawa}} = -\bar{Q}_L^T Y_{U,i} \tilde{\Phi}_i U_R - \bar{Q}_L^T Y_{D,i} \Phi_i D_R - \bar{L}_L^T Y_{L,i} \Phi_i E_R + \text{h.c.}, \quad (2.12)$$

with the three-dimensional Yukawa coupling matrices $Y_{\Psi,i}$ for the respective fermion triplet $\Psi \in \{U_L, D_L, E_L, N_L\}$ and the Higgs doublet Φ_i ($i \in \{1, 2\}$). The left-handed fermions are grouped into the doublets

$$Q_L = \begin{pmatrix} U_L \\ D_L \end{pmatrix} = \begin{pmatrix} (u_L, c_L, t_L)^T \\ (d_L, s_L, b_L)^T \end{pmatrix}, \quad L_L = \begin{pmatrix} N_L \\ E_L \end{pmatrix} = \begin{pmatrix} (\nu_{e,L}, \nu_{\mu,L}, \nu_{\tau,L})^T \\ (e_L, \mu_L, \tau_L)^T \end{pmatrix}, \quad (2.13)$$

and the right-handed fermion into the singlets

$$U_R = (u_R, c_R, t_R)^T, \quad D_R = (d_R, s_R, b_R)^T, \quad E_R = (e_R, \mu_R, \tau_R)^T. \quad (2.14)$$

The short-hand term $\tilde{\Phi}_k$ stands for $\epsilon_{ij} \Phi_k^*$ ($k \in \{1, 2\}$), where ϵ_{ij} is the totally antisymmetric tensor in two dimensions with

$$\epsilon_{ij} = \begin{pmatrix} 0 & 1 \\ -1 & 0 \end{pmatrix}. \quad (2.15)$$

In general, this allows flavour-changing neutral currents (FCNCs) at tree-level, because the Yukawa matrices are not necessarily diagonal in flavour space. Since FCNCs are not observed experimentally, they must be prevented in the theory, e.g., by imposing \mathbb{Z}_2 symmetries which force fermions of the same quantum numbers to only couple to one of the two Higgs doublets [30]¹. For a model with two $SU(2)_L$ doublets, there are four possibilities to realise such symmetries. In this work, we focus on the following one:

Type I 2HDM Imposing $\Phi_1 \rightarrow -\Phi_1$ (analogously to Eq. (2.4)) to the Yukawa sector, forces all quarks and leptons to couple only to the second Higgs doublet Φ_2 , and not the first doublet Φ_1 .

¹An alternative approach where FCNCs are naturally suppressed is the concept of minimal flavour violation [31–34].

3. The Dark Phases of the Next-to-Two-Higgs-Doublet Model

After EWSB, there are three phases in the N2HDM that provide one or more DM candidates, as introduced in Section 2.1. The IDP, in which $\mathbb{Z}_2^{(1)}$, Eq. (2.4), is non-broken and thus gives rise to three possible DM candidates; the DSP, where $\mathbb{Z}_2^{(2)}$, Eq. (2.5), is exact and which provides one neutral CP-even DM candidate; and the SM-like phase, where both \mathbb{Z}_2 symmetries remain unbroken. In this work, we focus on the IDP and the DSP, which are described in detail in Section 3.1 and 3.2, respectively.

3.1. The Inert Doublet Phase

In the IDP, only one of the two doublets acquires a non-vanishing VEV whilst the other doublet decouples from the SM particles. This configuration is only possible in the $\mathbb{Z}_2^{(1)}$ -conserving case of the potential for $m_{12}^2 = 0$. This gives rise to a conserved darkness parity that prevents the scalars of the inert doublet from decaying into SM particles and, therefore, the lightest of these dark scalars is a candidate for DM.

In the following, we diagonalise the scalar sector (Section 3.1.1) and reparametrise the potential in terms of physical parameters (Section 3.1.2). In Section 3.1.3, we summarise the resulting couplings of the mass eigenstates to SM particles. The triple-Higgs couplings are given in Appendix A.2.

3.1.1. Diagonalisation of the Scalar Sector

In this work, we assume without loss of generality the second doublet to be the SM-like doublet by choosing the following configuration of the VEVs after EWSB

$$\langle \Phi_1 \rangle = \begin{pmatrix} 0 \\ 0 \end{pmatrix}, \quad \langle \Phi_2 \rangle = \frac{1}{\sqrt{2}} \begin{pmatrix} 0 \\ v \end{pmatrix}, \quad \langle \Phi_S \rangle = v_s, \quad (3.1)$$

where v is the electroweak VEV with $v \approx 246$ GeV and the singlet VEV v_s is non-zero. This configuration provides the masses of fermions and gauge bosons as in the SM, while allowing for a mixing of the two neutral CP-even scalars ρ_2 and ρ_s . We parametrise this mixing in the mass eigenstates H_i ($i \in \{1, 2\}$) in terms of the mixing angle α by introducing

the following mixing matrix

$$\mathcal{R} = \begin{pmatrix} 0 & \cos \alpha & \sin \alpha \\ 0 & -\sin \alpha & \cos \alpha \\ 1 & 0 & 0 \end{pmatrix}. \quad (3.2)$$

By convention, we order the H_i by ascending mass

$$m_{H_1}^2 < m_{H_2}^2 \quad (3.3)$$

and choose the third mass eigenstate H_3 to be the dark scalar H_D . The neutral CP-odd and the charged sector are diagonalised by the usual 2HDM mixing matrix

$$\mathcal{U} = \begin{pmatrix} \cos \beta & \sin \beta \\ -\sin \beta & \cos \beta \end{pmatrix}. \quad (3.4)$$

Since $v_1 = 0$ and $v_2 = v$, $\sin \beta = 1$ and $\cos \beta = 0$ and, therefore,

$$G^0 = \eta_2, \quad A_D = -\eta_1, \quad (3.5)$$

$$G^\pm = \Phi_2^\pm, \quad H_D^\pm = -\Phi_1^\pm. \quad (3.6)$$

3.1.2. Parametrisation of the Potential in Terms of Physical Parameters

Exploiting the minimum conditions in Equations (2.8a)-(2.8c) and requiring the mass matrices to be diagonalised by the corresponding rotation matrices (3.2) and (3.4) allow the parameters of the potential to be expressed in terms of masses, VEVs and one mixing angle. The explicit parameter transformation is given in Appendix A.1. We call the parametrisation in terms of masses, VEVs and the mixing angle the *physical parametrisation* and the parametrisation in Eq. (2.3) with $m_{12}^2 = 0$ the *Lagrangian parametrisation*. The parameter sets of each basis are

$$\text{Lagrangian: } m_{11}^2, m_{22}^2, m_s^2, \lambda_1 - \lambda_8, \quad (3.7)$$

$$\text{Physical: } m_{11}^2, v, v_s, m_{H_1}, m_{H_2}, m_{H_D}, m_{A_D}, m_{H_D^\pm}, \quad (3.8)$$

$$\alpha, \lambda_1, \lambda_7.$$

The parameters m_{11}^2, λ_1 and λ_7 appear in both bases, because the Lagrangian contains a total of eleven real independent parameters, but there are only eight VEVs, masses and mixing angles. Therefore, these three parameters cannot be expressed in terms of physical parameters.

3.1.3. Higgs Couplings to SM Particles

Concerning the couplings to SM particles, we distinguish the *visible sector* consisting of the two neutral CP-even fields H_1 and H_2 (Section 3.1.3.1) and the *dark sector* including the three scalars H_D , A_D and H_D^\pm (Section 3.1.3.2). In the following, we give effective couplings

$$c(H_i(p)) = \frac{\lambda_i^{(p)}}{\lambda_{SM}^{(p)}} \quad (3.9)$$

of the scalar H_i ($i \in \{1, 2\}$) to a set of SM particles p normalised to the SM value, provided that there is a corresponding coupling in the SM. λ stands for the Feynman rule of the corresponding vertex and the division is taken to cancel identical tensor structures.

3.1.3.1. The Visible Sector

The visible sector of the IDP corresponds to the SM extended by a real singlet. Therefore, the effective couplings of H_1 and H_2 to a pair of fermions or a pair of gauge bosons is given by the $\mathcal{R}_{i,2}$ element of the mixing matrix in Eq. (3.2). These fulfil the sum rule

$$\sum_{i=1}^2 c^2(H_i \bar{f} f) = \sum_{i=1}^2 c^2(H_i V V) = 1. \quad (3.10)$$

Therefore, the couplings of the H_i cannot exceed the corresponding SM value. Furthermore, no FCNCs can occur since only the second doublet couples to fermions.

3.1.3.2. The Dark Sector

All couplings of the dark scalars H_D^\pm , H_D and A_D to a pair of fermions or a pair of gauge bosons vanish because of the preserved $\mathbb{Z}_2^{(1)}$ symmetry. However, two dark scalars can couple to a single vector boson, which allows – together with the triple-Higgs couplings $H_i H_D H_D$, $H_i A_D A_D$ and $H_i H_D^\pm H_D^\mp$ – to distinguish the IDP from a simple singlet extension of the SM. This type of coupling is dependent on the momenta of the scalars and there is no SM equivalent with which it could be normalised. We adopt the convention used in the Higgs Hunter’s Guide [25], in which the momentum p_{H_D} of H_D is incoming, and the momenta p_{A_D} and $p_{H_D^\pm}$ of the scalars A_D or H_D^\pm are outgoing. The resulting Feynman rules are

$$\lambda^\mu(H_D, A_D, Z) = -\frac{\sqrt{g^2 + g'^2}}{2} (p_{A_D} + p_{H_D})^\mu, \quad (3.11)$$

$$\lambda^\mu(H_D, H_D^\pm, W^\mp) = \mp \frac{ig}{2} (p_{H_D^\pm} + p_{H_D})^\mu. \quad (3.12)$$

The Feynman rules for the vertices $A_D H_D^\pm W^\mp$, $H_D^\pm H_D^\mp Z$ and $H_D^\pm H_D^\mp \gamma$ are the same as in the 2HDM and can be found in [25].

3.2. The Dark Singlet Phase

In the DSP, both doublets acquire non-zero VEVs but the singlet VEV vanishes, which leaves $\mathbb{Z}_2^{(2)}$, Eq. (2.5), unbroken. Thus, there is no mixing of ρ_s with the other scalar CP-even fields ρ_1 and ρ_2 . This and the fact that the singlet does not couple to SM particles makes ρ_s a DM candidate.

In the following, we describe the diagonalisation of the scalar sector in Section 3.2.1 and the reparametrisation of the potential in terms of physical parameters in Section 3.2.2. Then, we summarise the couplings to SM particles for a type I 2HDM and the triple-Higgs couplings in Section 3.2.3.

3.2.1. Diagonalisation of the Scalar Sector

Since the singlet does not acquire a VEV, we choose the usual configuration of the minima from the 2HDM

$$\langle \Phi_1 \rangle = \frac{1}{\sqrt{2}} \begin{pmatrix} 0 \\ v_1 \end{pmatrix}, \quad \langle \Phi_2 \rangle = \frac{1}{\sqrt{2}} \begin{pmatrix} 0 \\ v_2 \end{pmatrix}, \quad \langle \Phi_S \rangle = 0, \quad (3.13)$$

where $v_1 = v \cos \beta$ and $v_2 = v \sin \beta$ with the electroweak VEV $v \approx 246$ GeV. For compatibility with the 2HDM, we choose the following scalar mixing matrix

$$\mathcal{R} = \begin{pmatrix} -\sin \alpha & \cos \alpha & 0 \\ \cos \alpha & \sin \alpha & 0 \\ 0 & 0 & 1 \end{pmatrix}, \quad (3.14)$$

Table 3.1.: Effective Yukawa and gauge boson couplings of the CP-even Higgs bosons H_i ($i \in \{1, 2\}$) in the DSP normalised to the SM value, assuming a type I 2HDM [26].

	$c(H_i \bar{f} f)$	$c(H_i VV)$
H_1	$\cos \alpha / \sin \beta$	$-\sin(\alpha - \beta)$
H_2	$\sin \alpha / \sin \beta$	$\cos(\alpha - \beta)$

where we use the mass ordering

$$m_{H_1}^2 < m_{H_2}^2. \quad (3.15)$$

H_3 is taken as dark scalar H_D . The mixing matrix in Eq. (3.4) is used for the diagonalisation of the charged and neutral CP-odd sectors, which yields

$$G^0 = \eta_1 \cos \beta + \eta_2 \sin \beta, \quad A = -\eta_1 \sin \beta + \eta_2 \cos \beta, \quad (3.16)$$

$$G^\pm = \Phi_1^\pm \cos \beta + \Phi_2^\pm \sin \beta, \quad H^\pm = -\Phi_1^\pm \sin \beta + \Phi_2^\pm \cos \beta. \quad (3.17)$$

3.2.2. Parametrisation of the Potential in Terms of Physical Parameters

Analogously to Section 3.1, we use Eqs. (2.8a)-(2.8c) to trade m_{11}^2 and m_{22}^2 for v and $\tan \beta = \frac{v_2}{v_1}$. Requiring the mixing matrices in Eqs. (3.4) and (3.14) to diagonalise the mass matrices allows to express m_s^2 and λ_1 - λ_5 in terms of the masses and the mixing angle α . The explicit transformation of the parameters can be found in Appendix B.1. Since the parameter set of VEVs, masses and mixing angles, also called *physical parametrisation*, only consists of eight parameters but the Lagrangian consists of twelve real parameters, four Lagrangian parameters cannot be expressed in terms of physical parameters. Thus, the two sets of parametrisations read

$$\text{Lagrangian: } m_{11}^2, m_{22}^2, m_{12}^2, m_s^2, \lambda_1 - \lambda_8, \quad (3.18)$$

$$\text{Physical: } v, \tan \beta, m_{12}^2, m_{H_1}, m_{H_2}, m_{H_D}, m_A, m_{H^\pm}, \alpha, \lambda_6 - \lambda_8. \quad (3.19)$$

3.2.3. Higgs Couplings

Since the singlet field ρ_s neither couples to SM particles nor mixes with the other CP-even scalar fields ρ_1 and ρ_2 , the couplings of H_1 and H_2 to SM particles do not differ from the 2HDM and can be found in Table 3.1.

The only additional couplings compared to the 2HDM are the triple-Higgs couplings $H_i H_D H_D$ ($i \in \{1, 2\}$), which allow the decay of the light and heavy CP-even Higgs boson into DM if kinematically allowed, or vice versa the annihilation of two dark Higgs bosons into one light or heavy Higgs boson. The coupling for this interaction is given by

$$g(H_i H_D H_D) = \frac{\partial \mathcal{L}}{\partial H_i \partial H_D \partial H_D} = \lambda_7 v \cos \beta \cdot \mathcal{R}_{i1} + \lambda_8 v \sin \beta \cdot \mathcal{R}_{i2}, \quad (3.20)$$

where \mathcal{R}_{ij} is the ij element of the mixing matrix in Eq. (3.14).

4. Theoretical and Experimental Constraints

In order to decide whether a point of the IDP or the DSP with a given set of parameters is physical – i.e. that it agrees with theoretical requirements and experimental measurements – we impose certain conditions on the parameters of the potential or dependent quantities.

In Section 4.1, we begin with a description of the constraints resulting from the requirement for stability of the physical vacuum. Next, we specify the conditions applied to ensure compliance with perturbative unitarity at tree level. To ensure consistency with the discovery of a Higgs boson at the Large Hadron Collider (LHC) in 2012 [1,2], we demand that one of the CP-even Higgs bosons has a mass of 125.09 GeV [35]. In addition, we require its signal strengths to lie within the experimental bounds as described in Section 4.3. Since no additional Higgs bosons have been detected so far, we verify the agreement with experimental exclusion bounds from the Large Electron-Positron Collider (LEP), the Tevatron and the LHC using HiggsBounds 4.3.1 [36] and check for compliance with electroweak precision measurements as described in Section 4.4. In the DSP, we apply additional flavour constraints due to the direct coupling of the charged Higgs boson to fermions, see Section 4.5. We note that flavour constraints do not apply to the IDP, since the charged Higgs boson in this model does not couple to fermions. Concerning the dark sectors, we apply bounds resulting from cosmological DM observations and direct detection measurements as described in Section 4.6.

4.1. Vacuum Stability

Because of the rich vacuum structure of the N2HDM, a CP- and charge-conserving vacuum of the potential is not necessarily stable. To provide a stable vacuum, we check that the potential is bounded from below (Section 4.1.1) and that it does not decay into a deeper minimum as described in Section 4.1.2.

4.1.1. Conditions for the Potential to be Bounded from Below

In order to ensure that the potential has a global minimum at finite field values, we rely on the condition that the potential must be bounded from below, i.e. that it is positive for large field values. The necessary and sufficient conditions for the potential to be bounded from below have been derived in [37]. These restrict the parameters to the region

$$\Omega_1 \cup \Omega_2 \tag{4.1}$$

in parameter space, with

$$\Omega_1 = \left\{ \lambda_1, \lambda_2, \lambda_6 > 0; \lambda_7 + \sqrt{\lambda_1 \lambda_6} > 0; \lambda_8 + \sqrt{\lambda_2 \lambda_6} > 0; \right. \\ \left. D + \sqrt{\lambda_1 \lambda_2} > 0; \lambda_7 + \lambda_8 \sqrt{\frac{\lambda_1}{\lambda_2}} \geq 0 \right\}, \quad (4.2)$$

$$\Omega_2 = \left\{ \lambda_1, \lambda_2, \lambda_6 > 0; \sqrt{\lambda_2 \lambda_6} \geq \lambda_8 > -\sqrt{\lambda_2 \lambda_6}; -\lambda_8 \sqrt{\frac{\lambda_1}{\lambda_2}} \geq \lambda_7 > -\sqrt{\lambda_1 \lambda_6}; \right. \\ \left. D \lambda_6 > \lambda_7 \lambda_8 - \sqrt{(\lambda_7^2 - \lambda_1 \lambda_6)(\lambda_8^2 - \lambda_2 \lambda_6)} \right\}, \quad (4.3)$$

where the discriminant D is given by

$$D = \begin{cases} \lambda_3 & \text{for } \lambda_4 \geq |\lambda_5|, \\ \lambda_3 + \lambda_4 - |\lambda_5| & \text{for } \lambda_4 < |\lambda_5|. \end{cases} \quad (4.4)$$

4.1.2. Vacuum Decay and Global Minimum Conditions

Provided that the vacuum of the scalar potential is not the global minimum, it is possible that the vacuum tunnels into the deeper global minimum [38, 39]. Since the universe has already existed for more than 13 billion years, and none of the consequences of such a tunnelling have been observed, one condition for a potential parameter configuration is that its physical vacuum does not tunnel into a deeper minimum. This condition is met if the physical vacuum is the global minimum of the scalar potential. In general, it does not need to be the global minimum as long as the tunnelling time to a deeper minimum is larger than the age of the universe. However, as the calculation of the tunnelling time goes beyond the scope of this work, we do not consider metastable vacua, but rely on the stricter criterion that the minimum must be the global one.

To determine whether the vacuum is the global minimum, we follow the procedure of [23, 40], where the necessary conditions have already been derived for $m_{12}^2 \neq 0$. The case of $m_{12}^2 = 0$ leads to great simplifications, which we present in the following. First of all, we determine all possible minima of the scalar potential (see Eq. (2.3)) by setting up the stationary conditions for the most general field configuration

$$\Phi_1 = \frac{1}{\sqrt{2}} \begin{pmatrix} \varphi_1 + i \cdot \varphi_2 \\ \rho_1 + i \cdot \eta_1 \end{pmatrix}, \quad \Phi_2 = \frac{1}{\sqrt{2}} \begin{pmatrix} \varphi_3 + i \cdot \varphi_4 \\ \rho_2 + i \cdot \eta_2 \end{pmatrix}, \quad \Phi_S = \rho_s, \quad (4.5)$$

and the corresponding static field configuration

$$\langle \Phi_1 \rangle = \frac{1}{\sqrt{2}} \begin{pmatrix} 0 \\ v_1 \end{pmatrix}, \quad \langle \Phi_2 \rangle = \frac{1}{\sqrt{2}} \begin{pmatrix} v_{\text{cb}} \\ v_2 + i \cdot v_{\text{cp}} \end{pmatrix}, \quad \langle \Phi_S \rangle = v_s, \quad (4.6)$$

where v_{cb} and v_{cp} are the charge and CP breaking VEVs, respectively. Any other possible static field configuration of the N2HDM can be projected onto Eq. (4.6) by a gauge

transformation. The seven resulting non-trivial stationary conditions are

$$\left\langle \frac{dV}{d\varphi_1} \right\rangle = 0 \Leftrightarrow 0 = v_1 v_2 v_{cb} (\lambda_4 + \lambda_5), \quad (4.7a)$$

$$\left\langle \frac{dV}{d\varphi_2} \right\rangle = 0 \Leftrightarrow 0 = v_1 v_{cb} v_{cp} (-\lambda_4 + \lambda_5), \quad (4.7b)$$

$$\left\langle \frac{dV}{d\varphi_3} \right\rangle = 0 \Leftrightarrow -v_{cb} m_{22}^2 = \frac{1}{2} v_{cb} (v_1^2 \lambda_3 + v_2^2 \lambda_2 + v_{cb}^2 \lambda_2 + v_{cp}^2 \lambda_2 + v_s^2 \lambda_8), \quad (4.7c)$$

$$\left\langle \frac{dV}{d\rho_1} \right\rangle = 0 \Leftrightarrow -v_1 m_{11}^2 = \frac{1}{2} v_1 (v_1^2 \lambda_1 + v_2^2 \lambda_{345} + v_{cb}^2 \lambda_3 + v_{cp}^2 \lambda_{34-5} + v_s^2 \lambda_7), \quad (4.7d)$$

$$\left\langle \frac{dV}{d\rho_2} \right\rangle = 0 \Leftrightarrow -v_2 m_{22}^2 = \frac{1}{2} v_2 (v_1^2 \lambda_{345} + v_2^2 \lambda_2 + v_{cb}^2 \lambda_2 + v_{cp}^2 \lambda_2 + v_s^2 \lambda_8), \quad (4.7e)$$

$$\left\langle \frac{dV}{d\eta_1} \right\rangle = 0 \Leftrightarrow 0 = v_1 v_2 v_{cp} \lambda_5, \quad (4.7f)$$

$$\left\langle \frac{dV}{d\eta_2} \right\rangle = 0 \Leftrightarrow -v_{cp} m_{22}^2 = \frac{1}{2} v_{cp} (v_1^2 \lambda_{34-5} + v_2^2 \lambda_2 + v_{cb}^2 \lambda_2 + v_{cp}^2 \lambda_2 + v_s^2 \lambda_8), \quad (4.7g)$$

$$\left\langle \frac{dV}{d\rho_s} \right\rangle = 0 \Leftrightarrow -v_s m_s^2 = \frac{1}{2} v_s (v_1^2 \lambda_7 + v_2^2 \lambda_8 + v_{cb}^2 \lambda_8 + v_{cp}^2 \lambda_8 + v_s^2 \lambda_6), \quad (4.7h)$$

where we introduce the following shorthand terms for the combinations of the λ_i

$$\lambda_{345} = \lambda_3 + \lambda_4 + \lambda_5, \quad (4.8a)$$

$$\lambda_{34-5} = \lambda_3 + \lambda_4 - \lambda_5. \quad (4.8b)$$

The conditions (4.7a), (4.7b) and (4.7f) lead to three special cases. If we assume different combinations of non-zero v_1, v_2, v_{cb} and v_{cp} , we obtain

$$(4.7a) \quad \xrightarrow{v_1, v_2, v_{cb} \neq 0} \lambda_4 + \lambda_5 = 0, \quad (4.9)$$

$$(4.7b) \quad \xrightarrow{v_1, v_{cb}, v_{cp} \neq 0} \lambda_4 - \lambda_5 = 0, \quad (4.10)$$

$$(4.7f) \quad \xrightarrow{v_1, v_2, v_{cp} \neq 0} \lambda_5 = 0. \quad (4.11)$$

An additional case forcing $\lambda_4 = \lambda_5 = 0$ is obtained by assuming all four VEVs to be non-vanishing. Since this is only a special case of Eq. (4.10), this case does not further constrain the parameter space and therefore does not need to be considered separately. Except for the three cases (4.9)-(4.11), which are summarised in Table 4.1, v_1, v_2 and v_{cb}, v_1, v_{cb} and v_{cp} as well as v_1, v_2 and v_{cp} cannot be simultaneously non-zero. All other possible configurations are listed in Tables 4.2 and 4.3. Next, the formulae of the scalar potential for all of these cases are derived in terms of the Lagrangian parameters. In addition, the fact that all VEVs are real-valued leads to positivity conditions of the squared VEVs, which determine whether the corresponding case exists for a certain set of Lagrangian parameters. To determine whether the vacuum is the global minimum, we compare its value of the scalar potential to the values of all occurring stationary points. We do not check whether the respective cases are minima, maxima or saddle points. A detailed description of the procedure can be found in Appendix C.

4.2. Tree-Level Perturbative Unitarity

Perturbative unitarity at tree level is an important constraint for the parameter space region resulting from S-matrix unitarity [41]. For the considered models, we use the general numerical approach described in [28] to calculate all scalar quartic interaction amplitudes and construct the $2 \rightarrow 2$ scattering matrix. Unitarity of the scattering matrix is ensured by imposing an upper bound of 8π on the eigenvalues.

Table 4.1.: Special cases of vanishing (0) and non-vanishing (1) VEVs. The cases (s)IIa only exist if $\lambda_5 = 0$, (s)IIb if $\lambda_5 = -\lambda_4$ and (s)IVb if $\lambda_5 = \lambda_4$.

Case	IIa	IIb	IVb	sIIa	sIIb	sIVb
v_1	1	1	1	1	1	1
v_2	1	1	0	1	1	0
v_{cp}	1	0	1	1	0	1
v_{cb}	0	1	1	0	1	1
v_s	0	0	0	1	1	1

Table 4.2.: Overview over possible cases of vanishing (0) or non-vanishing (1) VEVs for $v_s = 0$. The cases IIa+b and IVb only exist for certain parameter configurations and are therefore shown in Table 4.1. Case nomenclature according to [23].

Case	I	IIIa	IIIb	IIIc	IVa	IVc	IVd	Va	Vb	Vc	Vd
v_1	1	0	0	0	1	1	1	0	0	0	0
v_2	1	0	0	0	0	0	0	1	1	1	1
v_{cp}	0	1	1	0	0	1	0	0	1	1	0
v_{cb}	0	1	0	1	0	0	1	0	1	0	1

Table 4.3.: Possible cases of vanishing (0) and non-vanishing (1) VEVs with $v_s \neq 0$. Analogously to Table 4.2, the cases sIIa+b and sIVb only exist for certain parameter configurations and are shown in Table 4.1.

Case	sI	sIIIa	sIIIb	sIIIc	sIVa	sIVc	sIVd	sVa	sVb	sVc	sVd	s
v_1	1	0	0	0	1	1	1	0	0	0	0	0
v_2	1	0	0	0	0	0	0	1	1	1	1	0
v_{cp}	0	1	1	0	0	1	0	0	1	1	0	0
v_{cb}	0	1	0	1	0	0	1	0	1	0	1	0

4.3. Signal Strengths of the h_{125}

Considering the LHC data on the Higgs boson, it is necessary to meet the signal strength of the h_{125} resulting from the combination of production and decay. We use the definitions from [42] for μ_F and μ_V , which are the Higgs boson production cross sections normalised to the SM. The first one,

$$\mu_F = \frac{\sigma(\text{ggH}) + \sigma(\text{bbH})}{\sigma_{\text{SM}}(\text{ggH}) + \sigma_{\text{SM}}(\text{bbH})}, \quad (4.12)$$

entails the sum of cross sections of the gluon fusion (ggH) and b -quark fusion (bbH) production channels normalised to the corresponding SM value. The included quantum-chromodynamics (QCD) corrections are described in Section 5.2.1. The second one is given by

$$\mu_V = \frac{\sigma(\text{VBF})}{\sigma_{\text{SM}}(\text{VBF})} = \frac{\sigma(\text{VH})}{\sigma_{\text{SM}}(\text{VH})} = c^2(H_i VV), \quad (4.13)$$

where $\sigma(\text{VBF})$ ($\sigma(\text{VH})$) is the production cross sections of the considered model via vector-boson fusion (vector-boson associated production) and $\sigma_{\text{SM}}(\text{VBF})$ ($\sigma_{\text{SM}}(\text{VH})$) is the corresponding SM value. QCD corrections cancel in the normalisation.

For each decay channel XX with $X \in \{\gamma, Z, W^\pm, b, \tau\}$ the signal strength is given by

$$\mu_{XX} = \mu_F \frac{BR(h_{125} \rightarrow XX)}{(BR(h_{125} \rightarrow XX))_{\text{SM}}}. \quad (4.14)$$

In order to agree with the experiment, we demand that each of the six quantities

$$\frac{\mu_F}{\mu_V}, \mu_{\gamma\gamma}, \mu_{ZZ}, \mu_{WW}, \mu_{bb}, \mu_{\tau\tau}, \quad (4.15)$$

is within $\pm(2 \times 1\sigma)$ of the respective experimental fit value [42].

4.4. Electroweak Precision Measurements

One of the most restrictive constraints on models beyond the SM is the ρ parameter. In the SM it is given by

$$\rho = \frac{m_W^2}{m_Z^2 \cdot \cos^2 \theta_W}, \quad (4.16)$$

where θ_W is the weak mixing angle and m_W and m_Z are the masses of the gauge bosons W^\pm and Z^0 , respectively, and indicates the relative strength of neutral and charged-current interactions in processes with four fermions and zero momentum transfer [8]. Therefore, it equals to one at tree-level. When adding only $SU(2)$ doublets with hypercharge $\pm\frac{1}{2}$ or $SU(2)$ singlets with zero hypercharge the ρ parameter remains unity at tree-level. At one-loop level, however, vacuum-polarization effects occur that lead to deviations from the SM value since in BSM theories additional fields couple to the W^\pm or Z^0 boson. These effects of BSM physics can be parametrised in terms of the so-called oblique parameters S , T and U [43]. We compute these parameters according to [44, 45] and demand a 2σ compatibility with the SM fit [46].

4.5. B-Physics Measurements

The presence of a non-dark charged Higgs boson in the DSP introduces a charged current, which can be revealed in the decay rates of K , D and B mesons. The most important constraint in this context comes from the rare decay $B \rightarrow X_s \gamma$. In this context, we apply the combined limits on m_{H^\pm} and $\tan\beta$ from [47, 48]. Furthermore, the charged Higgs boson contributes virtually to the one-loop process $Z \rightarrow b\bar{b}$. Here, we apply the constraint from [49] on the observable R_b .

4.6. Dark Matter Relic Density and Direct Detection

The main motivation for the investigated models is to provide appropriate candidates for DM. In order to determine whether the DM candidate for given set of parameters is suitable, we demand compatibility with measurements of the relic density and DM direct detection.

The latest measurements of the relic density of cold DM Ω_c in the Universe originate from the Planck observatory [4–6], a space telescope that mapped anisotropies in the cosmic microwave background radiation. We verify agreement by demanding the relic density to lie within or below the $2 \times 1\sigma$ band of the experimental fit value

$$\Omega_c h^2 = 0.1186 \pm 0.0020. \quad (4.17)$$

This excludes all parameter points that would lead to an over-abundance of DM in the Universe. Points that correspond to a lower value of the relic density than the value resulting from the Planck measurements remain viable, because the deficit in DM could be filled by a DM candidate arising from a different sector.

Regarding DM direct detection, we take into account the latest results provided by the XENON1T observatory, a dual phase (liquid-gas) xenon time projection chamber, dated November 2017 [50]. Since no DM nucleon scattering has been detected so far, an exclusion curve for the scattering cross section is obtained as a function of the mass of the dark particle. We fit a function

$$f_n(x) = \sum_{i=0}^{n+1} \frac{a_n}{x^{n-1}}, \quad (4.18)$$

with $x = M_{\text{LDP}}/\text{GeV}$ and $n = 6$ as shown in Figure 4.1, to the 90% C.L. exclusion bound on the spin-independent WIMP-nucleon cross section given in [50]. M_{LDP} is the mass of the lightest dark particle in a particular model. We use the resulting function,

$$\begin{aligned} \frac{\sigma_{\max}(M_{\text{LDP}})}{[\text{cm}^2]} &= 1.3048 \times 10^{-48} \frac{M_{\text{LDP}}}{\text{GeV}} + 1.3794 \times 10^{-48} \\ &\quad - 2.0759 \times 10^{-45} \frac{\text{GeV}}{M_{\text{LDP}}} + 3.8581 \times 10^{-43} \left(\frac{\text{GeV}}{M_{\text{LDP}}} \right)^2 \\ &\quad - 1.9211 \times 10^{-41} \left(\frac{\text{GeV}}{M_{\text{LDP}}} \right)^3 + 4.5806 \times 10^{-40} \left(\frac{\text{GeV}}{M_{\text{LDP}}} \right)^4 \\ &\quad - 4.9704 \times 10^{-39} \left(\frac{\text{GeV}}{M_{\text{LDP}}} \right)^5 + 2.1467 \times 10^{-38} \left(\frac{\text{GeV}}{M_{\text{LDP}}} \right)^6, \end{aligned} \quad (4.19)$$

to verify compatibility with constraints from direct detection. The XENON1T bound relies on a relic density equal to Eq. (4.17). Since we allow for smaller relic densities, the impact of the DM abundance on direct detection measurements is taken into account by considering a normalised scattering cross section $\hat{\sigma}_{\text{DM-N}}$ which is given by

$$\hat{\sigma}_{\text{DM-N}} = \sigma_{\text{DM-N}} \cdot \frac{\Omega_c h^2}{(\Omega_c h^2)_{\text{exp}}}, \quad (4.20)$$

where $\sigma_{\text{DM-N}}$ and $\Omega_c h^2$ are the values calculated for a given parameter set. In consequence, we demand that

$$\hat{\sigma}_{\text{DM-N}} \leq \sigma_{\max}(M_{\text{LDP}}). \quad (4.21)$$

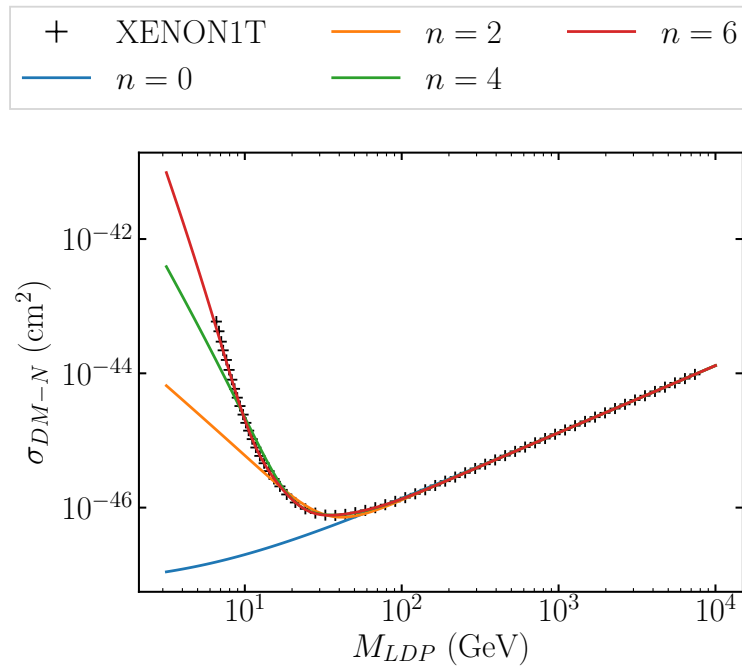


Figure 4.1.: Exclusion curve for the DM nucleon scattering cross section. The data points (black cross) are extracted from [50] and represent the 90% C.L. exclusion bound on the WIMP-nucleon cross section. The solid lines show the fit functions f_n (see Eq. (4.18)) for different n .

5. Scans of the Parameter Space

To compare the IDP and the DSP of the N2HDM, we perform random scans of the parameter space and calculate dependent quantities. The used tools are described in Section 5.1. In Section 5.2, we specify the features of the generated samples for both phases.

5.1. Description of the Used Tools

For the generation of parameter sets and the application of theoretical and experimental constraints, we use the **ScannerS** framework [28], which is presented in Section 5.1.1. **MicrOMEGAs 4.3.5** [51–53] (see Section 5.1.2) is used for the calculation of quantities related to the dark sector of each N2HDM phase.

5.1.1. ScannerS

ScannerS is a tool dedicated to perform scans of the parameter space of models with an extended scalar sector. Its approach is to avoid non-linear equations by using the VEVs, the masses of the Higgs bosons and the mixing matrix elements (e. g., the parameters sets (3.8) and (3.19) for the IDP and DSP, respectively) to scan over instead of the Lagrangian parameters (e. g., parameter sets (3.7) and (3.18)). For each parameter point that is generated **ScannerS** performs the following procedure [28]. First of all, uniformly distributed random values for the VEVs are chosen based on the symmetry-breaking pattern of the model. The requirement that the generated VEVs must be stationary points of the potential leads to a set of stationary conditions that allow to trade a subset of Lagrangian parameters for the VEVs. Next, the stationary points are demanded to be minima of the potential by assuming non-negative mass squares. The resulting quadratic derivative conditions link the remaining Lagrangian parameters to the physical masses and the matrix elements of the tree-level scalar mixing matrix. The latter are generated uniformly with respect to the Haar measure [54]. The independent parameters of the model are determined by solving the system of linear equations composed of the stationary and minimum conditions for fixed VEVs and mixing matrix elements. Then, uniformly distributed random values are generated for these parameters and the dependent parameters are calculated. Based on the complete set of parameters, **ScannerS** allows to test various conditions. In this context, all limits specified by the user are checked. Furthermore, the program includes a model-independent routine to test tree-level perturbative unitarity on a numerical basis, whereas the check for the potential to be bounded from below and the global minimum conditions must be defined when implementing the respective model. Constraints from null

searches for additional Higgs bosons at collider experiments are applied via an interface to `HiggsBounds` 4.3. Further constraints such as compliance with the signal strengths of the observed Higgs boson or limits from B physics are defined by the user.

5.1.2. MicrOMEGAs

The `MicrOMEGAs` framework [51–53] calculates the relic density as well as the rates for direct and indirect DM detection of a generic particle physics model involving cold DM. The underlying assumption is that the lightest DM candidate is stable due to a discrete symmetry, such as one of the \mathbb{Z}_2 symmetries introduced in Eqs. (2.4) and (2.5), which gives rise to a dark parity. This parity is even for all standard and additional visible particles and odd for the DM candidates. The implementation of a new model in `micrOMEGAs` is done by providing the `CalcHEP` [55] files that specify the basic quantities and all necessary relations. The generation of the required `CalcHEP` files is provided by `SARAH` [56].

5.2. The Samples of Parameter Points

In this section, we describe the steps taken to generate a large number of physical parameter sets for the respective models. Therefore, we present the implementations for `ScannerS` and `micrOMEGAs` in Section 5.2.1 and specify the applied ranges for the input parameters in Section 5.2.2.

5.2.1. Basics of Sample Generation

For the investigation of the IDP and the DSP, we implement each model as separate `ScannerS` model class. For both models, the constraints arising from tree-level unitarity are applied via the built-in method, whereas the vacuum-stability constraints are implemented as described in the Sections 4.1.1 and 4.1.2. The check for compliance with the measured signal strengths of the h_{125} and the electroweak precision measurements are implemented as indicated in Sections 4.3 and 4.4, respectively. The cross sections for the production channels ggH and bbH are obtained via the `ScannerS` interface to `SusHi` 1.6.0 [57] at next-to-next-to-leading-order (NNLO) QCD. The branching ratios of the Higgs bosons, which are input parameters for the `HiggsBounds` routine, are calculated by interfacing `N2HDECAY` [23], which is a modified version of `HDECAY` 6.51 [58–60]. `N2HDECAY` calculates the Higgs boson branching ratios for the broken phase and the DSP including all QCD corrections available in `HDECAY`. We have extended the existing code to the IDP by adding the couplings specific for this phase (see Section 3.1). Electroweak corrections are not included in the parameter scans or the analysis as they are not available for the investigated models. The B -physics constraints applying to the DSP are taken over from the `ScannerS` implementation of the 2HDM since they only depend on the charged Higgs boson. Constraints from the measurement of the relic density and DM direct detection are not applied in `ScannerS` but these quantities are calculated separately via `micrOMEGAs`. Therefore, we implement both models in `SARAH` 4.12 and use its `CalcHep` interface to generate the model files for `micrOMEGAs`. In this routine, `SARAH` also provides a C++ code which we modify in such a way that it reads the values of the Lagrangian parameters of a given `ScannerS` point and calculates the corresponding relic density and nucleon scattering cross section.

5.2.2. Scan Ranges

In the IDP and the DSP, we use the parameter sets of Eqs. (3.8) and (3.19) as input parameters. For compatibility with the SM, we fix the VEV v to

$$v = \frac{1}{\sqrt{\sqrt{2}G_F}}, \quad (5.1)$$

where G_F is the Fermi coupling constant [5]. In addition, we demand one of the CP-even Higgs bosons to have a mass of

$$m_{h_{125}} = 125.09 \text{ GeV}. \quad (5.2)$$

The masses of the other Higgs bosons are allowed in the ranges

$$30 \text{ GeV} \leq m_{H_{\downarrow}}, m_{H_D}, m_{A_{(D)}}, m_{H_D^{\pm}} < 1 \text{ TeV}, \quad (5.3)$$

$$80 \text{ GeV} \leq m_{H_{\pm}} < 1 \text{ TeV}, \quad (5.4)$$

where $m_{H_{\downarrow}}$ denotes the second CP-even Higgs boson that can be either lighter or heavier than the h_{125} . Although charged DM as lightest dark particle is generally considered excluded, we keep the possibility of H_D^{\pm} being lighter than H_D and A_D in order to verify this statement in the IDP. However, we exclude Higgs bosons with masses in the ± 5 GeV interval around $m_{h_{125}}$ – except if the Higgs boson belongs to the dark sector – to avoid considering the superposition and interference effects of a degenerate Higgs signal. In the IDP, we vary v_s in the range

$$1 \text{ GeV} \leq v_s < 1.5 \text{ TeV}, \quad (5.5)$$

whereas in the DSP we allow for

$$0.1 \leq \tan \beta < 35. \quad (5.6)$$

Since the lower bound in $\tan \beta$ is below the threshold obtained by the constraint from $B \rightarrow X_s \gamma$, it has no influence on the physical parameter points. The mixing matrix elements generated by **ScannerS** are transformed in order to match with Eqs. (3.2) and (3.14) for the IDP and the DSP, respectively. Therefore the mixing angles of both phases are in the range

$$-\frac{\pi}{2} \leq \alpha < \frac{\pi}{2}. \quad (5.7)$$

In the IDP, we additionally need three of the Lagrangian parameters in order to obtain the full set of eleven parameters. These are the mass parameter m_{11}^2 , for which we allow for

$$-10^6 \text{ GeV}^2 \leq m_{11}^2 \leq 10^6 \text{ GeV}^2, \quad (5.8)$$

and the dimensionless parameters λ_1 and λ_7 . The latter are constrained by the conditions for the potential to be bounded from below (see Section 4.1.1) and the requirement for unitarity of the $2 \rightarrow 2$ scattering matrix described in Section 4.2. Therefore, the dimensionless parameters are generated in the intervals specified in Table 5.1¹. Since the limits from both constraints are stronger than the given minimum and maximum values, the given ranges do not further constrain the parameter space. In the DSP, the full set of parameters consists of twelve parameters, because in general the $\mathbb{Z}_2^{(1)}$ soft-breaking parameter m_{12}^2 is not set to zero, as required in the IDP. However, we also force

$$m_{12}^2 = 0 \quad (5.9)$$

in the DSP, as this facilitates comparing both models on the basis of the same number of free parameters. The dimensionless parameters $\lambda_6 - \lambda_8$ are allowed in the same ranges as in the IDP (see Table 5.1).

¹The limits on the dependent parameters are applied to save computing time, because these bounds are checked in first place. Thereby we avoid unnecessary further calculations if the point is excluded anyway by the constraints from tree-level perturbative unitarity or the requirement for the potential to be bounded from below.

Table 5.1.: Minimum and maximum values for the dimensionless parameters λ_{1-8} . These limits are applied regardless of the parameters being dependent or independent.

	λ_1	λ_2	λ_3	λ_4	λ_5	λ_6	λ_7	λ_8
min	0	0	-17	-17	-10	0	-26	-26
max	10	10	17	17	10	17	26	26

6. Phenomenological Results

In this chapter, we present the results of the parameter scans described in Chapter 5. In Sections 6.1-6.3, we scrutinise all points that are in agreement with theoretical requirements (see Sections 4.1-4.2) and constraints from collider experiments (see Sections 4.3-4.5) as well as the cosmological value of the relic density of DM (see Section 4.6). In Section 6.1 we begin by analysing the properties of the h_{125} and discuss how physical parameter points of our two N2HDM phases can deviate from SM expectations. In Section 6.2 we study the mass distributions of the additional scalars occurring in our N2HDM phases and compare these to similar models. In Section 6.3, we investigate the predictions for the measurement of an additional Higgs boson at collider experiments. We discuss the predicted cross sections and point out how to distinguish our phases through observation of a second Higgs boson. In the last section (6.4), we study the subset of points also fulfilling limits that arise from direct detection of DM (see Section 4.6) in order to investigate the impact of DM direct detection limits on the previously discussed quantities.

6.1. Properties of the h_{125}

In this section, we study the phenomenology of the h_{125} in terms of its admixtures. We define the singlet admixture Σ_i of the Higgs boson H_i in the IDP by

$$\Sigma_i^{\text{IDP}} := \mathcal{R}_{i3}^2. \quad (6.1)$$

In the DSP, we define the doublet admixture Δ_i

$$\Delta_i^{\text{DSP}} := \left(\frac{\mathcal{R}_{i2}}{\tan \beta} - \mathcal{R}_{i1} \right)^2, \quad (6.2)$$

since the CP-even Higgs bosons are given by

$$H_i = \frac{\mathcal{R}_{i2}}{\sin \beta} H_{\text{SM}} - \left(\frac{\mathcal{R}_{i2}}{\tan \beta} - \mathcal{R}_{i1} \right) \rho_1, \quad (6.3)$$

with $H_{\text{SM}} = \cos \beta \rho_1 + \sin \beta \rho_2$. In the following, the singlet admixture of the h_{125} in the IDP is simply referred to as Σ and the doublet admixture of the h_{125} in the DSP is simply referred to as Δ . In Section 6.1.1, we compare the two phases by means of the h_{125} couplings and discuss the influence of the respective admixtures. In Section 6.1.2, we focus on the signal strengths that can be measured at collider experiments.

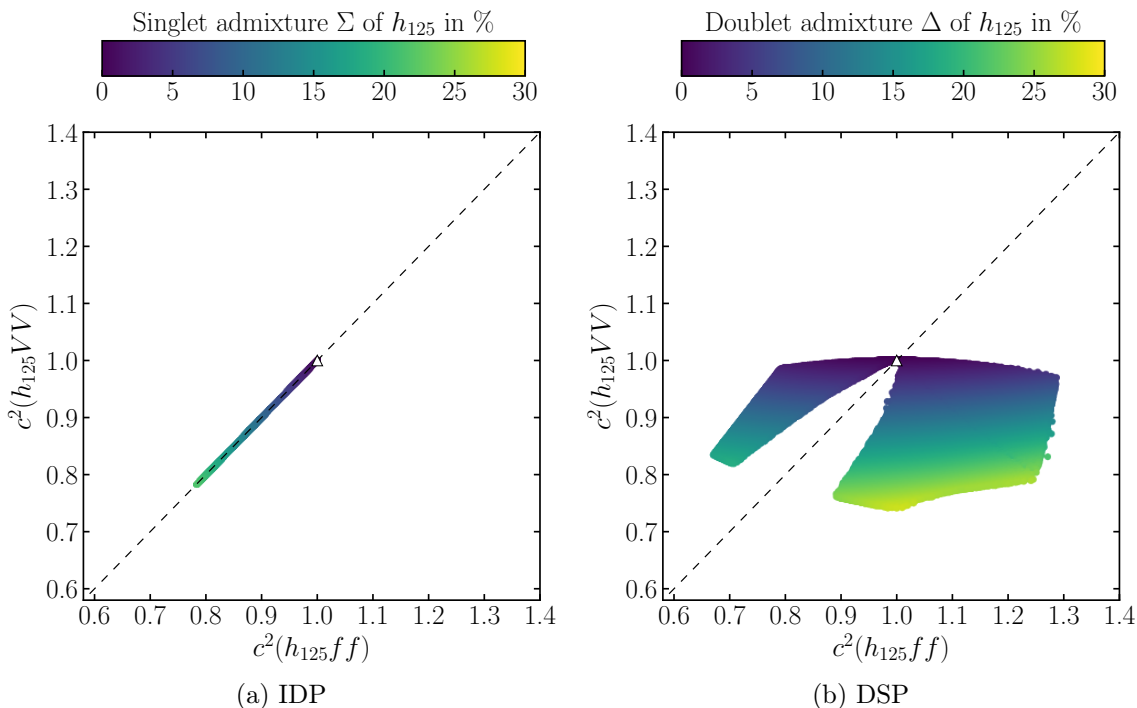


Figure 6.1.: Squared effective coupling of the h_{125} to a pair of vector bosons as a function of the squared effective coupling to a pair of fermions in the IDP (a) and the DSP (b). The dashed line corresponds to $c^2(h_{125}VV) = c^2(h_{125}ff)$ and the white triangle denotes the SM value. The colour code indicates the singlet or doublet admixture in the respective phase.

6.1.1. Couplings to SM Particles

The effective couplings of the h_{125} normalised to the SM value are given in Sections 3.1.3.1 and 3.2.3 for the IDP and DSP, respectively. We note, that in each of the phases, the effective coupling is the same for up-type and down-type quarks as well as for leptons. Figure 6.1 shows the distribution of the physical parameter points in terms of the couplings of h_{125} to a pair of vector bosons and a pair of fermions for the IDP (a) and the DSP (b). The colour code indicates the corresponding maximum singlet or doublet admixture corresponding to a certain coupling in the IDP or DSP, respectively.

In the IDP, the relation between these couplings is simply a straight line, because both depend on one common factor. The range of the couplings squared is constrained at the upper end by the sum rule given in Eq. (3.10) and at the lower end by the experimentally observed signal strengths of the h_{125} . The latter also constrains the maximum singlet admixture. Only values up to $\Sigma \approx 22\%$ are allowed, corresponding to effective couplings to SM particles of $c^2(h_{125}VV) = c^2(h_{125}ff) \approx 0.78$, because the singlet admixture fulfils the relation

$$\Sigma = 1 - c^2(h_{125}ff) = 1 - c^2(h_{125}VV). \quad (6.4)$$

Therefore, it decreases if the couplings tend to the SM value.

In the DSP, however, the relation between the coupling to vector bosons and the coupling to fermions is more complex, because the couplings do not only depend on the mixing angle α but also on β . Considering the couplings to fermions, this allows for a broader range that includes values above the SM value up to $c^2(h_{125}ff) \approx 1.29$. The upper and lower limits are obtained from the experimentally observed signal strengths of the h_{125} . Since

the couplings of the CP-even Higgs bosons fulfil the sum rule

$$\sum_{i=1}^2 c^2(H_i VV) = 1, \quad (6.5)$$

the coupling of the h_{125} to vector bosons cannot exceed the SM value. Its lower limit is caused by the requirement to fulfil the experimentally measured signal strengths of the vector boson decay channels ZZ and W^+W^- (see Section 6.1.2). The gap we observe at $c^2(h_{125}ff) \approx c^2(h_{125}VV)$ is due to trigonometric relations. Regarding the doublet admixture, small values correspond by construction to a SM-like coupling to vector bosons whereas the coupling decreases with increasing doublet admixture, because of the relation

$$\Delta = \frac{1 - c^2(h_{125}VV)}{\sin^2 \beta}. \quad (6.6)$$

The requirements on the signal strengths of the h_{125} allow for a doublet admixture of up to $\Delta \approx 30\%$. The coupling to fermions, on the other hand, does not show a significant dependency on the doublet admixture.

Comparing the two phases, we observe that the coupling to vector bosons hardly allows a discrimination. Both phases allow approximately the same coupling range and show similar characteristics regarding the impact of the singlet or doublet admixture on $c^2(h_{125}VV)$. In contrast to the IDP, however, the DSP provides a larger spectrum in terms of the coupling of h_{125} to fermions by allowing slightly smaller values, but also values well above the SM value.

6.1.2. Signal Strengths at Collider Experiments

In order to investigate the observable properties of the h_{125} , we use the six quantities

$$\frac{\mu_F}{\mu_V}, \mu_{\gamma\gamma}, \mu_{ZZ}, \mu_{WW}, \mu_{bb}, \mu_{\tau\tau}, \quad (6.7)$$

defined in Eqs. (4.12)-(4.14). Since both phases preserve custodial symmetry, we note that the signal strengths μ_{WW} and μ_{ZZ} are equal and thus define

$$\mu_{VV} := \mu_{WW} = \mu_{ZZ}. \quad (6.8)$$

Regarding the experimental limits on both quantities, we combine the $2 \times 1\sigma$ lower bound from μ_{ZZ} and the $2 \times 1\sigma$ upper bound from μ_{WW} to one constraint on μ_{VV} :

$$0.79 < \mu_{VV} < 1.48. \quad (6.9)$$

In addition, we observe that the experimental limits on the signal strength $\mu_{\tau\tau}$ are not sufficiently precise to constrain our phases, and therefore do not show this quantity¹.

Starting with the IDP, we show the four remaining signal strengths in Figure 6.2. We observe in Figure 6.2a, that this phase is constrained by the lower limit μ_{VV} , whereas the upper limit is given by the fact, that neither the couplings to vector bosons nor the couplings to fermions can exceed the SM value. Experimental limits on μ_{bb} do not further constrain the parameter space. Analogously to the couplings shown in Figure 6.1a, the relation between the fermion and the vector boson related signal strengths is a straight line. Likewise, low values of the singlet admixture correspond to signal strengths values close to the SM value and increasing values in Σ correspond to decreasing values in the

¹Note that the experimental limits on μ_{bb} are more constraining than the ones on $\mu_{\tau\tau}$ only because of an under fluctuation in the 7 – 8 TeV LHC data [35].

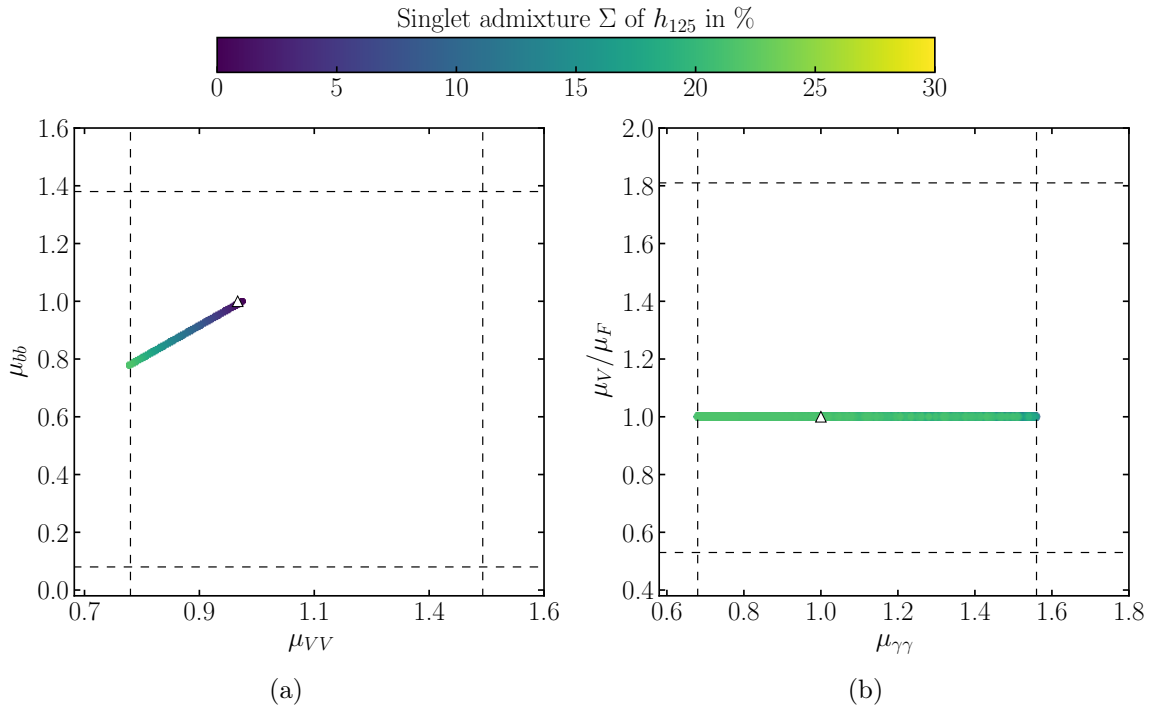


Figure 6.2.: Signal strengths of the h_{125} in the IDP normalised to the SM. (a) shows the signal strength for a pair of bottom quarks as a function of the vector-boson signal strength. In (b), the ratio of production through (ggH + bbH) and VBF is shown as a function of the photon signal strength. The colour code indicates the maximum singlet admixture to the h_{125} . The dashed lines show the experimental limits from [42] and the white triangle denotes the SM value.

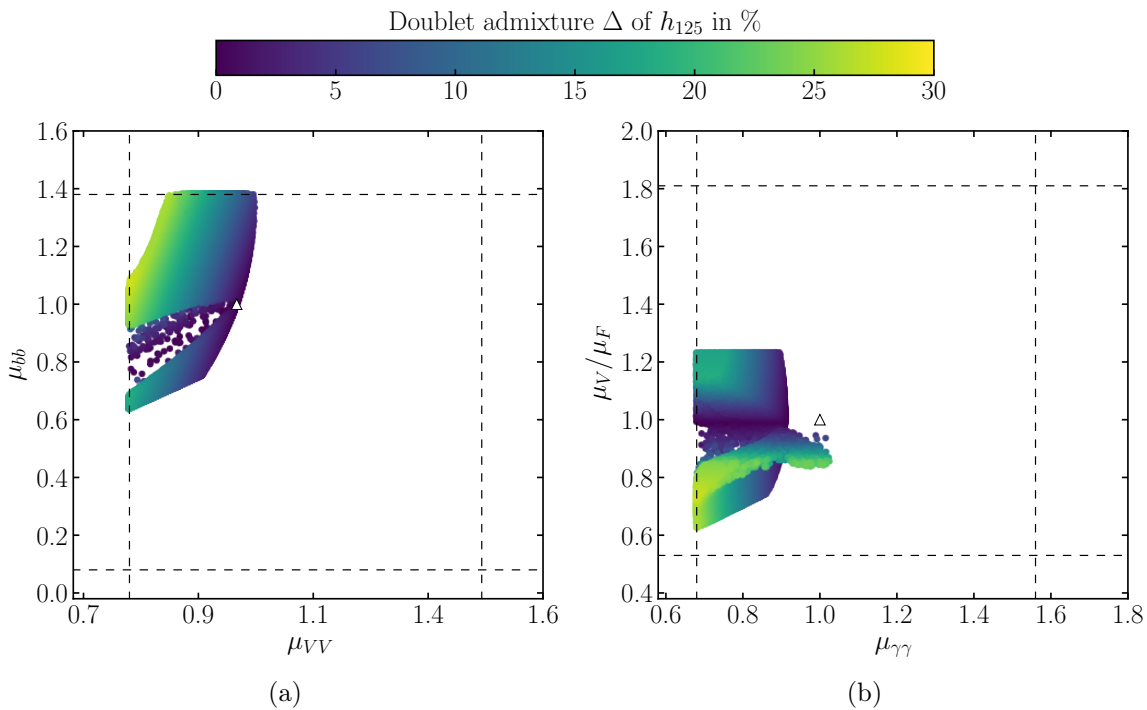


Figure 6.3.: Signal strengths of the h_{125} in the DSP normalised to the SM. (a) shows the signal strength for a pair of bottom quarks as a function of the vector-boson signal strength. In (b), the ratio of production through (ggH + bbH) and VBF is shown as a function of the photon signal strength. The colour code indicates the maximum doublet admixture to the h_{125} . The dashed lines show the experimental limits from [42] and the white triangle denotes the SM value.

signal strengths μ_{bb} and μ_{VV} . Figure 6.2b shows the distribution of points in the $\frac{\mu_V}{\mu_F} - \mu_{\gamma\gamma}$ plane. We find that the parameter space of the IDP is not constrained by the experimental limits on $\frac{\mu_V}{\mu_F}$ since the dependency of both quantities on the mixing angle α cancels in the normalisation and, therefore, the fraction $\frac{\mu_V}{\mu_F}$ equals to one by construction. However, the phase is constrained by both lower and upper limits in $\mu_{\gamma\gamma}$. In this channel an enhancement compared to the SM is possible, because of the one-loop contribution of the dark charged Higgs bosons – see Appendix A.2 for the triple-Higgs couplings. In the whole range of $\mu_{\gamma\gamma}$ the singlet admixture lies within 0%² to 22% and, therefore, a more precise measurement of the photon signal strength does not allow to constrain the singlet admixture.

Figure 6.3 shows the distribution of the points of the DSP in the signal-strength planes. As for the couplings, this phase provides a larger spectrum compared to the IDP. The lower bound on μ_{VV} , see Figure 6.3a, is set by its experimental limit whereas the upper bound is obtained through the maximum coupling to vector bosons given by the SM value. However, the vector-boson signal strength can exceed the corresponding SM value in combination with an enhanced coupling to fermions such as the top quark which provides the dominant contribution to the ggH production channel. This corresponds to the region $(\mu_{bb} > 1) \wedge (\mu_{VV} > 1)$. In the μ_{bb} direction the lower bound originates from a search for additional Higgs bosons³. The upper bound results from the $2 \times 1\sigma$ upper limit of the experimental measurements of μ_{bb} . The lower bound in μ_{VV} above $\mu_{bb} \approx 1.1$ is con-

²In Figure 6.2 smaller singlet admixtures are hidden behind points with larger singlet admixture.

³For each Higgs boson of the model, the `HiggsBounds` routine determines the most sensitive experimental search. In the region above $\frac{\mu_V}{\mu_F} \approx 1.3$, the most sensitive search for the h_{125} is a CMS analysis in the channel $pp \xrightarrow{\text{VBF}} H \rightarrow WW$ [61] that excludes parameter points with $c^2(h_{125}VV) \text{BR}(h_{125} \rightarrow W^+W^-) / \text{BR}_{\text{SM}}(h_{125} \rightarrow W^+W^-) \gtrsim 0.9$.

strained by measurements of the photonic signal strength. An enhanced signal strength in the $b\bar{b}$ decay channel corresponds to an enhanced coupling to all fermions and, therefore, an increase in the t -loop contribution to $h_{125} \rightarrow \gamma\gamma$. Since this contribution interferes destructively with the dominant W -loop contribution, the overall signal strength in the $\gamma\gamma$ channel decreases and is ruled out by the experimental lower limit. In order to be compatible with the lower limit of the photon signal strength, a parameter point with an enhanced coupling to fermions cannot have a simultaneously reduced coupling to vector bosons. Therefore, physical points with an enhanced μ_{bb} must also show an enhancement in μ_{VV} . Regarding the doublet admixture, we observe – analogously to the couplings in Figure 6.1b – that small doublet admixtures correspond by construction to vector boson signal strengths close to the SM value. This tendency is not reflected in the direction of the fermion signal strength. However, we observe doublet admixtures of up to $\Delta \approx 28\%$ for μ_{bb} above 0.9 and only $\Delta \approx 18\%$ below. Figure 6.3b shows the distribution of points in the $\frac{\mu_V}{\mu_F} - \mu_{\gamma\gamma}$ plane. We observe that the parameter space is constraint by the experimental lower bound of the photonic signal strength. The upper limit is $\mu_{\gamma\gamma} \approx 1.02$. However, the majority of points is well below $\mu_{\gamma\gamma} = 1$ and we do not observe any points at the SM value of $\frac{\mu_V}{\mu_F} = \mu_{\gamma\gamma} = 1$. This is a known feature of 2HDMs with $m_{12}^2 = 0$ [27]. In order to explain this behaviour, we consider the main contributions to the decay channel into $\gamma\gamma$ that are the two SM contributions via t and W^\pm loops as well as the BSM contribution via H^\pm loops. Regarding the SM contributions, the t -loop contribution, which interferes destructively with the W^\pm -loop contribution, can be enhanced due to the allowed fermion coupling range of up to $c^2(Hff) \approx 1.3$ whereas the W^\pm loop cannot since the maximum value of the effective coupling $c^2(HVV)$ is unity. Furthermore, the BSM contribution can, in general, interfere constructively or destructively with the SM contribution, depending on the sign of the triple-Higgs coupling $H_i H^+ H^-$. This coupling depends on the mass of the charged Higgs boson and – for the general DSP – on m_{12}^2 . The charged Higgs boson loop contributes increasingly destructive with increasing m_{H^\pm} whereas its interference becomes constructive for large m_{12}^2 . This compensation of large charged Higgs boson masses is not possible in our model, because we set $m_{12}^2 = 0$. In order to get within -5% (-9%) of the SM value in $\mu_{\gamma\gamma}$, we require $m_{H^\pm} \lesssim 95$ GeV (120 GeV). Regarding the ratio of the contributions to Higgs boson production, deviations from the SM value of $\frac{\mu_V}{\mu_F} = 1$ are possible with increasing doublet admixture. These are limited from below by the experimental upper limit of μ_{bb} . Values above $\frac{\mu_V}{\mu_F} \approx 1.3$ correspond to the excluded region in the $\mu_{bb} - \mu_{VV}$ plane at small μ_{bb} (see Figure 6.3a) and are therefore rejected by [61].

In conclusion, the DSP allows considerable room for deviations from the SM signal strengths in terms of diminished as well as enhanced signal rates in all but the photonic channel. In this decay channel, the SM value is only allowed for small charged Higgs boson masses. In contrary, the IDP does not allow for enhancements compared to the SM in any of the signal strengths but $\mu_{\gamma\gamma}$. The latter can take any value compatible with the experimental fit.

6.2. Mass Distributions of the Additional Scalars

In this section, we address the phenomenology of the additional Higgs bosons present in our phases. We begin by discussing the IDP that provides one additional visible Higgs boson. We note that its mass covers the whole input range of 30 GeV – 1 TeV. The corresponding dark sector consists of three scalars, the lightest of which is the DM candidate. The relation between the masses of these dark Higgs bosons is studied in Section 6.2.1. The DSP provides only one dark scalar whose physically allowed mass ranges from 30 GeV to 1 TeV. The corresponding visible sector is enlarged by one CP-even, one CP-odd and one charged Higgs boson. The distributions of the physically allowed masses of the visible Higgs bosons is studied in Section 6.2.2.

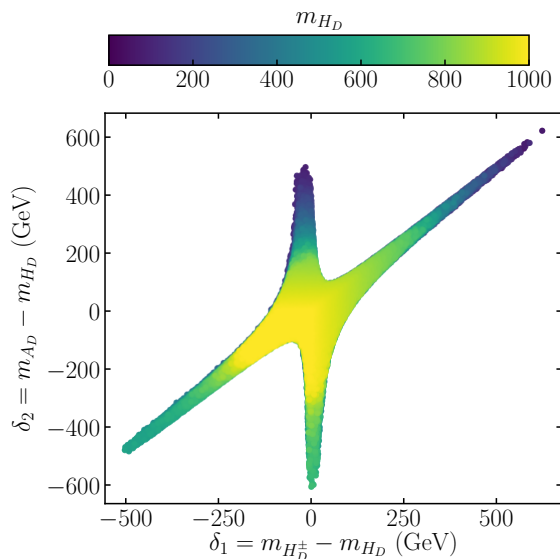


Figure 6.4.: IDP: Mass splitting δ_2 of the dark CP-odd and CP-even scalars as function of the mass splitting δ_1 of the dark charged and CP-even scalars. The colour bar represents the maximum mass of the dark CP-even Higgs boson for a given point in the δ_1 - δ_2 plane. To be compared to [62].

6.2.1. Mass Splittings of the Dark Scalars in the Inert Doublet Phase

In this section, we discuss the mass characteristics of the three dark scalars in the IDP. We note that constraints from searches for additional Higgs bosons do not apply to the dark sector of the IDP since these searches rely on decays into pairs of SM particles but H_D , A_D and H_D^\pm do not decay into pairs of SM particles⁴. The allowed mass ranges for the dark scalars are

$$30 \text{ GeV} \leq m_{H_D}, m_{A_D} < 1 \text{ TeV}, \quad (6.10a)$$

$$46 \text{ GeV} \leq m_{H_D^\pm} < 1 \text{ TeV}. \quad (6.10b)$$

The upper and lower bounds for the neutral scalars as well as the upper bound of the mass of the dark charged Higgs boson are given by the input scan ranges, whereas the lower bound in $m_{H_D^\pm}$ results from the requirement $2m_{H_D^\pm} > m_Z$. Off-shell decays of the Z boson into charged dark Higgs bosons are negligible because the charged dark Higgs boson is either stable or its decays $H_D^\pm \rightarrow W^\pm + H_D/A_D$ are phase-space suppressed. According to [62], we define the splittings between the masses of the charged and CP-odd Higgs bosons with respect to the mass of the CP-even Higgs boson

$$\delta_1 = m_{H_D^\pm} - m_{H_D}, \quad (6.11)$$

$$\delta_2 = m_{A_D} - m_{H_D}. \quad (6.12)$$

We observe that these splittings, see Figure 6.4, manifest in a characteristic shape. The legs formed by the physical parameters points lie essentially in two regions, one in which the mass splitting between the charged and the CP-even Higgs boson is less than 110 GeV (vertical legs) and the other in which the difference between the masses of the charged and the CP-odd Higgs boson is smaller than 70 GeV (diagonal legs). These legs meet where the mass splittings of all three dark Higgs bosons are less than 200 GeV. This relation is

⁴Searches for decays of a heavy dark Higgs boson into a lighter one and a vector boson are not included in `HiggsBounds 4.3`, but will be supported from `HiggsBounds 5` onwards.

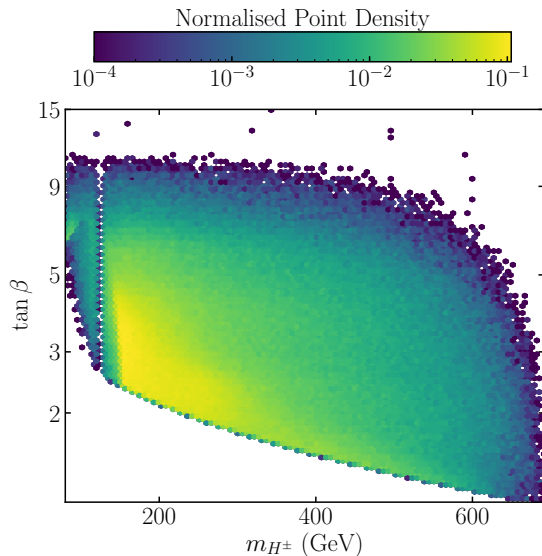


Figure 6.5.: DSP: Distribution of physical points in the plane of $\tan \beta$ and the charged Higgs boson mass. The colour code indicates the relative abundance of parameter points. The gap at m_{H^\pm} is due to the window we require around $m_{h_{125}}$.

well-known from the IDM [62] and originates from constraints of electroweak precision measurements because two of the dark scalars can couple to a single gauge boson and, therefore, contribute to the oblique parameters S and T . This means that in the IDM only parameter points are allowed for which either A_D (H_D^\pm) has a mass within $m_{H_D} \pm 110$ GeV (70 GeV) or both have masses within $m_{H_D} \pm 200$ GeV. For large masses of the dark CP-even Higgs boson ($m_{H_D} \gtrsim 900$ GeV), only parameter points that provide $(|\delta_1| < 200 \text{ GeV}) \wedge (|\delta_2| < 200 \text{ GeV})$ are in agreement with electroweak precision measurements.

6.2.2. Mass Ranges of the Visible Scalars in the Dark Singlet Phase

Regarding the masses of the additional visible scalars in the DSP, we observe the following ranges

$$30 \text{ GeV} \leq m_{H_\uparrow}, m_A < 700 \text{ GeV}, \quad (6.13a)$$

$$80 \text{ GeV} \leq m_{H^\pm} < 700 \text{ GeV}. \quad (6.13b)$$

While the lower limit on the masses is given by the input scan ranges, the upper limit arises from the fact, that for $m_{12}^2 = 0$ these masses only depend on $\lambda_1 - \lambda_5$, the mixing angle α and $\tan \beta$. The constraints on $\lambda_1 - \lambda_5$ by tree-level perturbative unitarity and the requirement for the potential to be bounded from below result in upper bounds for the masses of the Higgs bosons, see [27]. We observe in Figure 6.5 that the upper bound in the charged Higgs boson mass results in a lower bound in $\tan \beta$. This lower bound in $\tan \beta$, which decreases with increasing m_{H^\pm} arises due to exclusion limits from measurements of the rare decay $B \rightarrow X_s \gamma$ [47, 48]. The minimum value in our sample is $\tan \beta \approx 1.1$.

6.3. Distinguishing the Dark Phases Through the Properties of the Additional Higgs Bosons

In this section, we investigate how to distinguish between our two phases based on the assumption that an additional Higgs boson is discovered at the LHC. One of the first properties being determined is whether the discovered Higgs boson is a charged or a neutral state. The DSP would allow for both possibilities. On the contrary, the charged Higgs

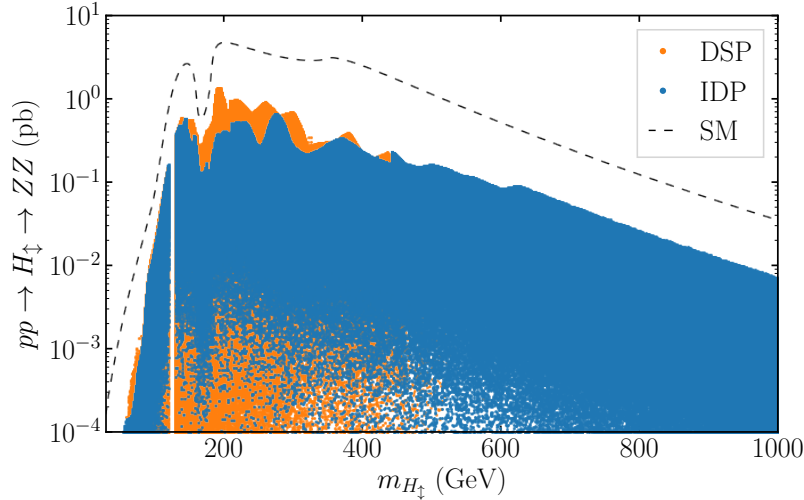


Figure 6.6.: Inclusive production and decay cross section for the decay channel $H_{\downarrow} \rightarrow ZZ$ as a function of the H_{\downarrow} mass. The IDP is shown in blue and the DSP in orange. The dashed black line corresponds to the cross section of a Higgs boson with SM-like couplings. The gap at 125 GeV is due to the window we exclude around $m_{h_{125}}$ (see Section 5.2.2).

boson in the IDP can only be produced in pairs and does not couple to fermions. Since this would be extremely difficult to measure, the discovery of a charged Higgs boson would rule out the IDP. Considering the discovered Higgs boson to be neutral, the state could either be CP-even, CP-odd or mixed. The latter is not possible in neither of our N2HDM phases and is thus not further discussed. The discovery of a CP-odd Higgs boson at collider experiments is not compatible with the IDP due to the same reasons as the discovery of a charged Higgs boson. However, both phases allow an additional visible CP-even Higgs boson H_{\downarrow} . In the following, we discuss how to distinguish between the two phases based on the respective predictions for the H_{\downarrow} properties. In order to discuss which kind of observations could or could not be explained by our phases, we investigate the inclusive production and decay rates for decays into various SM particles. The production cross section

$$\sigma(pp \rightarrow H_{\downarrow}) = \sigma(ggH) + \sigma(bbH) \quad (6.14)$$

is calculated via `SusHi` at NNLO QCD for a center-of-mass energy of 13 TeV using the effective fermion couplings of the respective phase. We neglect the minor contributions from vector boson fusion and associated production, because neither of our phases allow an enhancement in the coupling to vector bosons. The branching ratios are calculated via `N2HDECAY`.

First, we discuss the decay channel in ZZ whose production is shown in Figure 6.6 as a function of the H_{\downarrow} mass in the IDP and DSP in comparison to the SM-like reference. Due to the sum rule of the effective couplings

$$\sum_{i=1}^2 c^2(H_i VV) = 1, \quad (6.15)$$

neither of our phases allows for an enhanced gauge-boson coupling of the CP-even Higgs bosons compared to the SM. In addition, we require a large percentage of the gauge-boson coupling for h_{125} to agree with experimental observations in the ZZ and W^+W^- final states. This only allows for $c^2(H_{\downarrow} VV) \lesssim 0.27$ in the DSP and $c^2(H_{\downarrow} VV) \lesssim 0.22$ in the

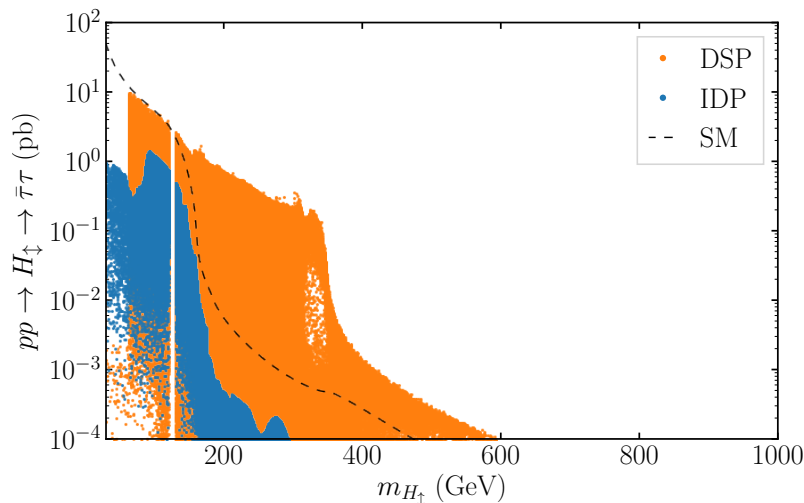


Figure 6.7.: Inclusive production and decay cross section for the decay channel $H_{\downarrow} \rightarrow \tau\tau$ as a function of the H_{\downarrow} mass. The dashed black line corresponds to the cross section predicted for a Higgs boson with SM-like couplings. The gap at 125 GeV is due to the window we exclude around $m_{h_{125}}$.

IDP. In order to compensate small gauge-boson couplings either an increased production or a reduced total width of the H_{\downarrow} is required. Increasing the production requires increasing the coupling of H_{\downarrow} to top quarks, whereas reducing the total width requires a reduction of, e.g. $\Gamma(H_{\downarrow} \rightarrow b\bar{b})$. Since $c^2(Ht\bar{t}) = c^2(Hb\bar{b})$ holds in both of our phases, any enhancement in the production would be compensated by an increase of the total width and vice versa. In conclusion, neither of the phases allows a cross section in the channel $pp \rightarrow H_{\downarrow} \rightarrow ZZ$ above the corresponding SM reference. In this channel, a discrimination between the two phases is hardly feasible because both show a very similar behaviour. Only a discovery of a Higgs boson with a mass above $m_{H_{\downarrow}} = 700$ GeV would clearly rule out the DSP, since it does not provide a CP-even Higgs boson in this mass range.

Regarding the leptonic decay channels of H_{\downarrow} , we examine the predictions for the $\tau\bar{\tau}$ decay channel shown in Figure 6.7. As mentioned in the above paragraph, the maximum value of the squared coupling of the H_{\downarrow} to vector bosons in the IDP is 0.22. Due to $c^2(H_i VV) = c^2(H_i ff)$, the rate of $pp \rightarrow H_{\downarrow} \rightarrow \tau\bar{\tau}$ in the IDP is always well below the SM reference for the same Higgs boson mass. In contrary, the sum rule applying to the fermion couplings in the DSP is

$$\sum_{i=1}^2 c^2(H_i f \bar{f}) = \frac{1}{\sin^2 \beta}. \quad (6.16)$$

which – in combination with the lower limit in $\tan \beta$ (see Section 6.2.2) – allows for parameter points with $c^2(H_{\downarrow} f \bar{f})$ up to 1. This allows the production via ggH to be comparable to the SM reference. A reduction of the branching ratio into ZZ allows for a considerably enhanced branching ratio into a pair of τ leptons and, therefore, an enhancement in the inclusive cross section compared to the SM reference. Hence, the discovery of a Higgs boson in the $\tau\bar{\tau}$ channel allows a discrimination of the two phases. For a Higgs boson mass below 63 GeV the IDP provides larger rates in the $\tau\bar{\tau}$ channel than the DSP. This is due to a combination of constraints on the signal strengths of the h_{125} and limits from **HiggsBounds**. In the range $63 \text{ GeV} < m_{H_{\downarrow}} < 125 \text{ GeV}$, the DSP allows for inclusive cross sections of an order of magnitude higher than the dark doublet phase. Above $m_{h_{125}}$, the cross section in the IDP drops – similar to the SM reference – due to the opening of decays into W^+W^- and, therefore, an additional Higgs boson would not be observable in the $\tau\bar{\tau}$

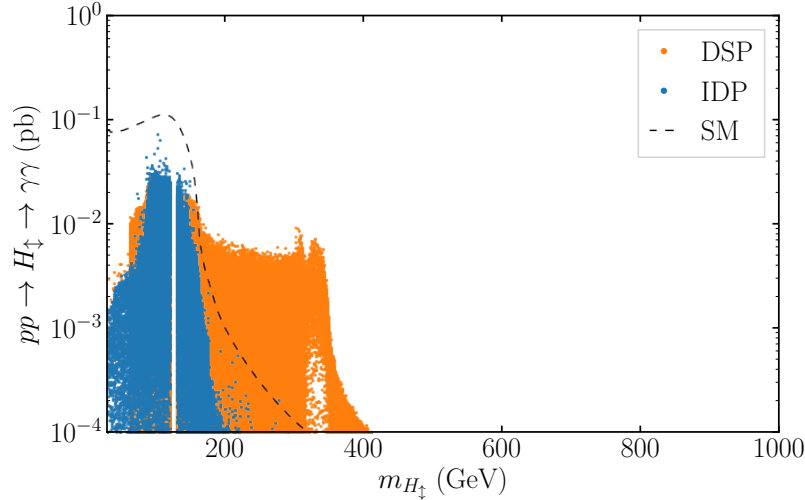


Figure 6.8.: Inclusive production and decay cross section for the decay channel $H_{\downarrow} \rightarrow \gamma\gamma$ as a function of the H_{\downarrow} mass. The dashed black line corresponds to the cross section for a Higgs boson with SM-like couplings. The gap at 125 GeV is due to the window we exclude around $m_{h_{125}}$.

channel. In the DSP, however, the rates remain high up to $m_{H_{\downarrow}} \approx 350$ GeV, where the decay into a pair of top quarks becomes dominant.

We conclude this part of the analysis by studying the decay channel $H_{\downarrow} \rightarrow \gamma\gamma$ whose inclusive cross section is shown in Figure 6.8. The production cross section is again limited by the maximum value of $c^2(H_{\downarrow}ff)$ in the respective phase whereas the branching ratio contains the loop contributions of W bosons, t quarks and the charged Higgs bosons. Thus, in the IDP the production cross section is reduced compared to the SM reference whereas the DSP allows for a H_{\downarrow} production cross section comparable to the SM reference. In the IDP, the SM contributions from W and t loops are modified by the effective couplings, which is the same factor for both contributions. As stated above, the maximum value the effective coupling can take is $c^2(H_{\downarrow}VV) = c^2(H_{\downarrow}f\bar{f}) = 0.22$. The charged-Higgs contribution can interfere constructively with the SM contributions which allows for an enhancement of the photonic rate. However, the low production cross section and small SM contributions cannot be compensated by the BSM contribution and therefore the inclusive production and decay cross section in the IDP does not exceed the SM reference. In the DSP, the W -loop contribution is suppressed because of $c^2(H_{\downarrow}VV) \lesssim 0.27$. Since this restriction does not apply to fermions, the squared fermion coupling $c^2(H_{\downarrow}ff)$ can reach values of up to ≤ 1 and, therefore, the t -loop contribution can become dominant. In combination with sufficiently large top couplings and a reduced total width due to a decrease in $\Gamma(H_{\downarrow} \rightarrow ZZ/W^+W^-)$, the DSP allows for a considerable enhancement in the $pp \rightarrow H_{\downarrow} \rightarrow \gamma\gamma$ inclusive cross section compared to the SM reference. In the region $m_{H_{\downarrow}} < 125$ GeV – similarly to the $\tau\bar{\tau}$ channel – the inclusive cross sections of both phases are smaller than the SM reference. However, in this channel, the cross sections for both phases are of the same order of magnitude. For heavier H_{\downarrow} , the cross section $pp \rightarrow H_{\downarrow} \rightarrow \gamma\gamma$ for the IDP is predicted to drop, whereas the one for the DSP remains at the same level up to $m_{H_{\downarrow}} \approx 2m_t$, where the decay channel into two on-shell top quarks opens.

In summary, it is difficult to distinguish between the two phases solely on the basis of inclusive cross sections. However, a discovery of a second Higgs boson with a mass above 700 GeV – regardless of the decay channel – would exclude the DSP. Nor could the discovery of a very light Higgs boson ($m_H \lesssim 60$ GeV) in the channel $\tau\bar{\tau}$ be explained by the DSP. Similarly, the discovery of a Higgs boson with a mass of more than 200 GeV and a rate of

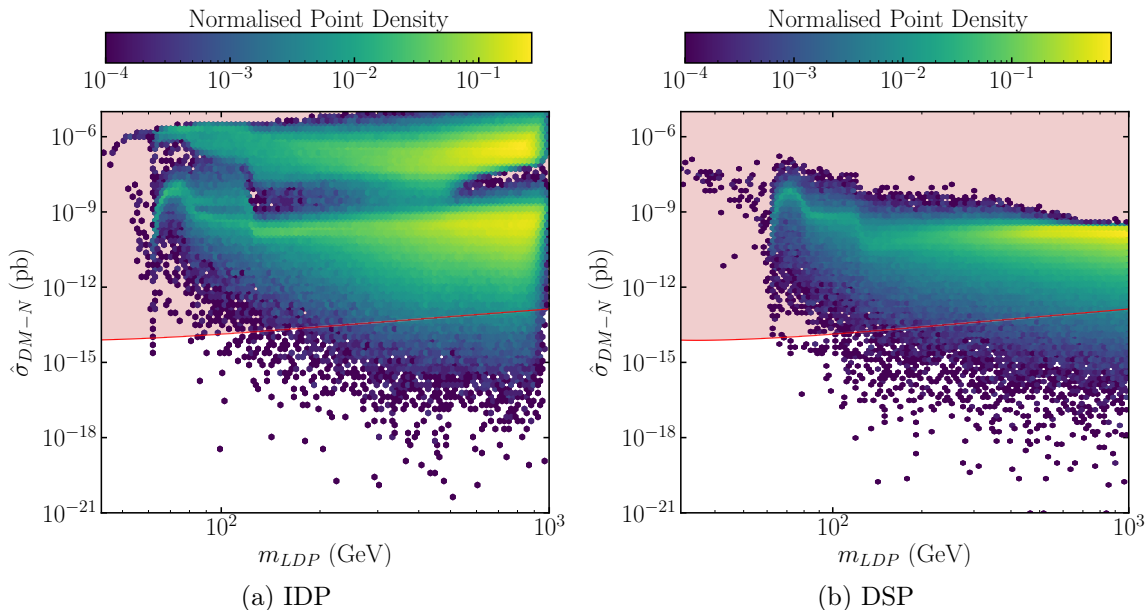


Figure 6.9.: Normalised spin-independent dark-matter-nucleon-scattering cross section according to Eq. (4.20) plotted over the mass of lightest dark particle in the respective phase. The red line corresponds to the exclusion bound from the XENON1T observatory [50].

about 10 fb in the $\gamma\gamma$ channel or 100 fb in the $\tau\tau$ channel would put the IDP under strain.

6.4. The Impact of Dark Matter Direct Detection Constraints

Since the above considerations include all constraints except those resulting from the direct detection of DM, this section analyses how these additional constraints (see Section 4.6) affect the parameter space of our two phases. We start in Section 6.4.1 by analysing the distribution of parameter points in the plane of the DM nucleon cross section and the mass of the lightest dark particle. In Section 6.4.2, we discuss the impact of the DM direct detection exclusion bound on the quantities of the visible sector discussed in Sections 6.1-6.3 and finally examine the allowed ranges of the DM masses and the relic density predicted by the IDP and DSP, see Section 6.4.3.

6.4.1. Dark Matter Nucleon Cross Sections

In Figure 6.9 the distribution of the whole samples of the two phases is shown in the plane of the DM nucleon cross section and the mass of the lightest dark particle. In the IDP (a), we observe two distinct regions that contain the majority of points. The region with larger DM nucleon cross sections ($\hat{\sigma} \gtrsim 1 \times 10^{-8}$ pb) corresponds to points with the charged Higgs boson as lightest dark particle. The lower region ($\hat{\sigma} \lesssim 1 \times 10^{-8}$ pb) is populated with points whose lightest dark particle is H_D or A_D . Since the DSP (b) only provides one CP-even DM candidate, the distribution of parameter points resembles the ones in the IDP with H_D or A_D as lightest dark particle. We observe that the exclusion bound from the XENON1T experiment [50] rules out a vast majority of points in both phases. In the DSP, 0.83% of the sample is compatible with the exclusion bound. In the IDP only 0.73% are compatible, because parameter points with H_D^\pm as lightest dark particle generally correspond to larger scattering cross sections than points with H_D or A_D as lightest dark particle. Thus, all of the parameter points with H_D^\pm as lightest dark particle are ruled out by the XENON1T exclusion bound.

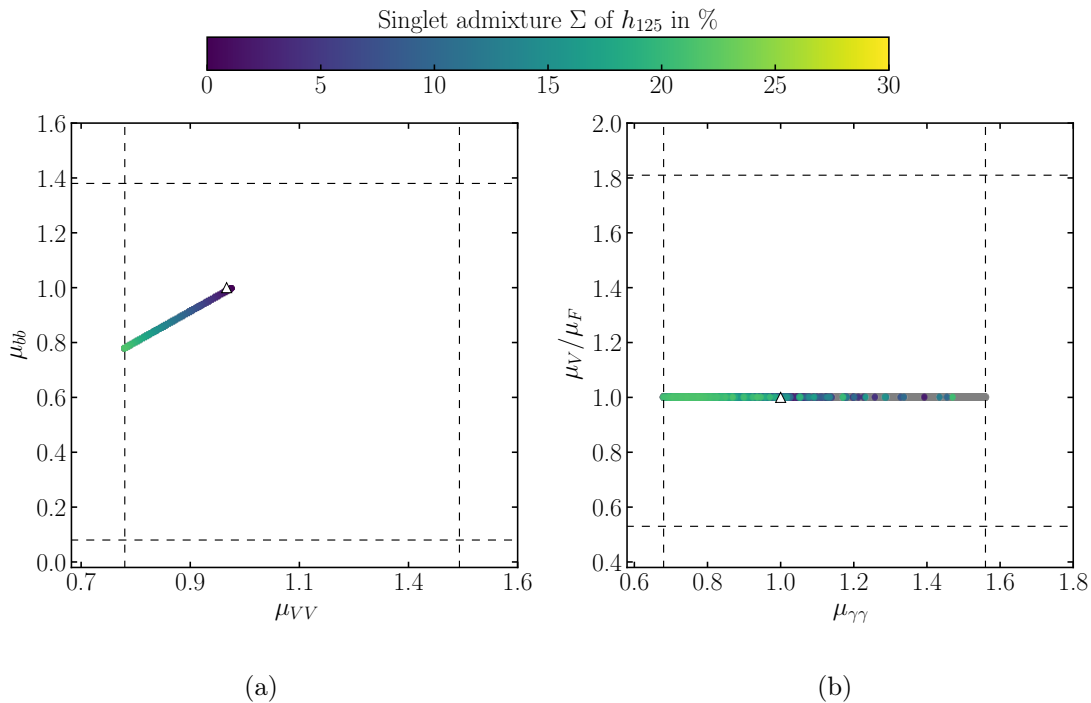


Figure 6.10.: Signal strengths of the h_{125} in the IDP normalised to the SM as in Figure 6.2. The colour-coded points are those that fulfil the direct detection constraints, the entire sample is shaded in grey. The dashed lines show the experimental limits from [42] and the white triangle denotes the SM value.

6.4.2. The Impact on the Visible Sector

Since the visible and dark sectors of both phases are only linked via the triple and quartic Higgs couplings, we would expect no significant impact of DM direct detection constraints on the visible sector. In order to check this assumption, we take a second look at the signal strengths of the h_{125} . Figures 6.10 and 6.11 show the distribution of parameter points of the IDP and DSP, respectively, which are compatible with the direct detection constraints. To compare with Figures 6.2 and 6.3, the distributions of the entire samples are shown in grey. In the IDP, we observe that in the μ_{bb} - μ_{VV} plane the distribution of parameter points compatible with the direct detection constraints lies exactly above the distribution of the entire sample. In the $\frac{\mu_V}{\mu_F}$ - $\mu_{\gamma\gamma}$ plane, we observe the same effect in the range of $\mu_{\gamma\gamma} \leq 1$. Above $\mu_{\gamma\gamma} = 1$ there are fewer points, nevertheless values up to $\mu_{\gamma\gamma} \approx 1.5$ are reached. We suspect that this is simply the result of lower statistics. However, this must be further studied in future work. We further note that the allowed range for the singlet admixture remains the same as in the entire sample. In the DSP, we equally observe that the distribution of parameter points fulfilling direct detection constraints is mostly similar to that of the entire sample. However, there are a few relatively empty regions in the μ_{bb} - μ_{VV} and in the $\frac{\mu_V}{\mu_F}$ - $\mu_{\gamma\gamma}$ plane. This is most likely due to statistical effects and has to be further investigated in future work. Regarding the inclusive production and decay cross sections of H_{\downarrow} , we similarly observe no different distributions than in the Figures 6.6-6.8. We thus conclude that DM direct detection bounds do not have a significant impact on the visible sector.

6.4.3. The Impact on the Dark Sector

We observe from the distributions in Figure 6.9, that in both phases very light DM candidates are excluded by direct detection constraints. The allowed mass ranges for the three

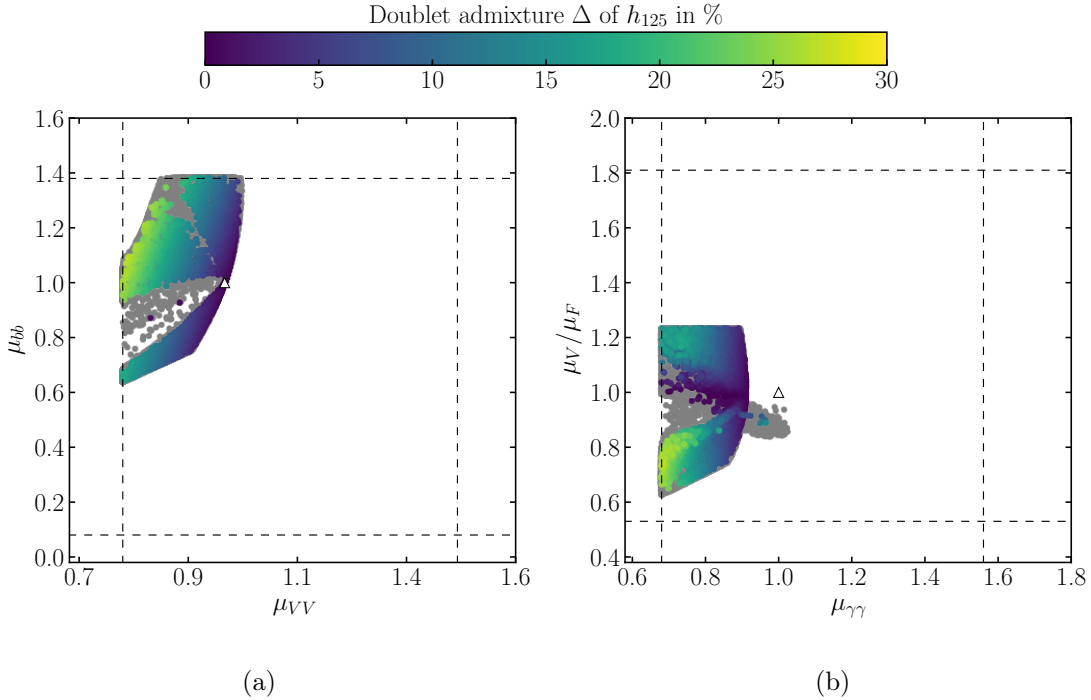


Figure 6.11.: Signal strengths of the h_{125} in the DSP normalised to the SM as in Figure 6.3. The colour-coded points are those that fulfil the direct detection constraints, the entire sample is shaded in grey. The dashed lines show the experimental limits from [42] and the white triangle denotes the SM value.

DM candidates in the IDP are

$$61 \text{ GeV} \leq m_{H_D}, m_{A_D} < 1 \text{ TeV}, \quad (6.17a)$$

$$78 \text{ GeV} \leq m_{H_D^\pm} < 1 \text{ TeV}. \quad (6.17b)$$

As shown in Figure 6.12, the direct detection constraints exclude the charged Higgs boson as lightest dark particle. For $\delta_2 > 0$, δ_1 is strictly positive, i.e. if the CP-odd dark Higgs boson is heavier than the CP-even one, the charged dark Higgs boson cannot be lighter than H_D without being excluded by DM direct detection. Similarly, if A_D is lighter than H_D , $|\delta_1|$ must always be smaller than $|\delta_2|$ for the charged dark Higgs boson not to be the lightest dark particle. Otherwise, the statements in section 6.2.1 remain valid. In the DSP, dark Higgs bosons in the mass range

$$65 \text{ GeV} \leq m_{H_D} < 1 \text{ TeV} \quad (6.18)$$

can be realised.

Finally, we investigate how successfully the two phases can reproduce the observed relic density. We therefore plot the relic densities realised in our two phases over the mass of the respective lightest dark particle, see Figure 6.13. We observe that both phases generally allow for relic densities of $\mathcal{O}(10^{-8})$ up to $\mathcal{O}(10^2)$. In the IDP, the cosmological value is achieved for either DM masses below 110 GeV or above 720 GeV. The DSP allows to realise the cosmological value in the whole mass range $30 \text{ GeV} \leq m_{\text{LDP}} \leq 1 \text{ TeV}$. Regarding the subset of parameter points that fulfil DM direct detection constraints, Figure 6.13a shows that the maximum DM relic density realised in the IDP is an order of magnitude below the cosmological value. Therefore, in the range $30 \text{ GeV} \leq m_{\text{LDP}} \leq 1 \text{ TeV}$ the IDP by itself is not sufficient to explain the observed abundance of DM, but another source of DM

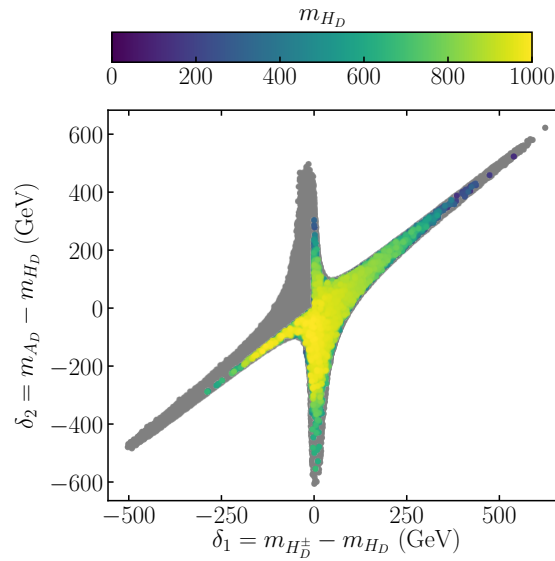


Figure 6.12.: IDP: Mass splitting δ_2 of the dark CP-odd and CP-even scalars as function of the mass splitting δ_1 of the dark charged and CP-even scalars. The coloured points are the ones fulfilling direct detection constraints. The colour code denotes the mass of H_D . The whole sample is shown in grey.

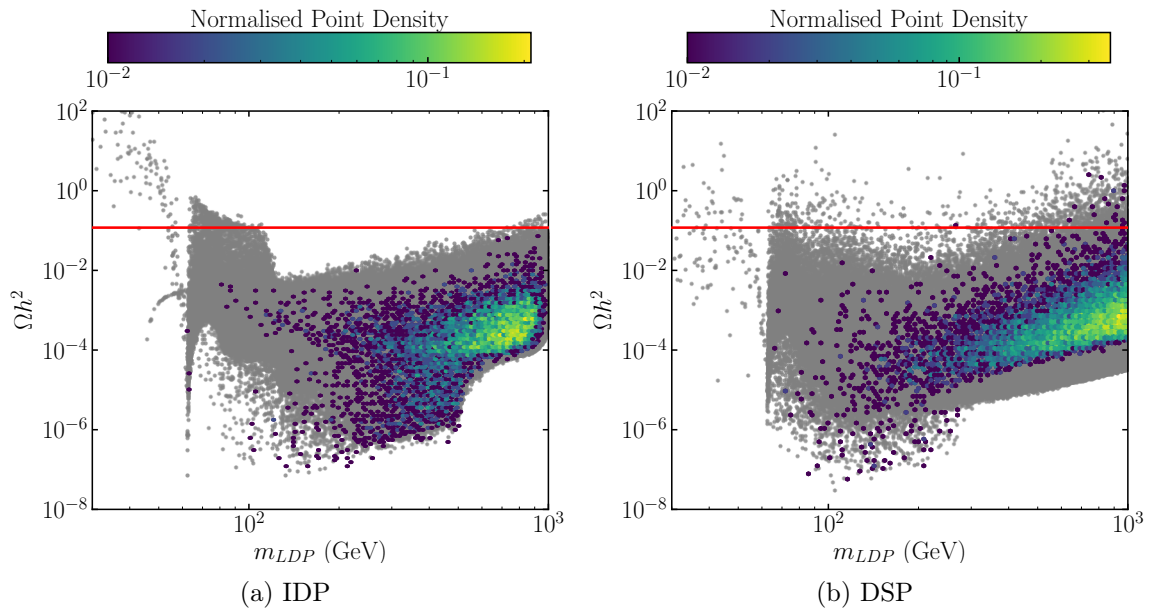


Figure 6.13.: Distribution of the DM relic density as a function of the mass of the lightest dark particle in the respective model. The coloured points are the ones fulfilling the direct detection constraints, where the colour code corresponds to the density of parameter points. The grey points correspond to the entire sample. The red line corresponds to the $2 \times 1\sigma$ region around the cosmological value of the relic density [4–6].

would be necessary. In the DSP, see Figure 6.13b, we observe parameter points with relic density values both above and below the cosmological value. While parameter points with a DM relic density above the cosmological value are not physical, because they lead to an abundance of DM, the DSP can also provide scenarios that reproduce the observed relic density.

7. Conclusion

In this work we compared two of the simplest extensions of the SM providing a WIMP as DM candidate, namely doublet and singlet DM. We selected the N2HDM because it allows both approaches to be implemented as two different phases of EWSB based on one common scalar sector. The IDP and the DSP both provide one additional neutral CP-even Higgs boson that can mix with the 125 GeV state. The IDP further provides three dark Higgs bosons – one neutral CP-even, one neutral CP-odd and one charged state. The DSP only provides one neutral CP-even DM candidate, whereas the neutral CP-odd and charged states are part of the visible sector. In this work, we focus on the \mathbb{Z}_2 -conserving potential and couplings to fermions as in a type I 2HDM.

In order to investigate the two phases, we performed an extensive parameter scan of each phase using the **ScannerS** framework. We implemented each phase as a **ScannerS** model class and applied all relevant theoretical and experimental constraints. This includes checks for vacuum stability and tree-level perturbative unitarity as well as collider constraints applying to the 125 GeV or the other visible states of the respective phase. In the DSP, due to presence of a non-dark charged Higgs boson, we included additional constraints from B -physics measurements. Constraints on the dark sectors are not applied within the **ScannerS** framework but the relic density as well as the nucleon-scattering cross section are calculated separately using **micrOMEGAs**. Based on this procedure, we generated samples with physical parameter points that allow to study the properties of the visible and dark sectors of each phase.

Regarding the visible sector, we scrutinised the phenomenology of the 125 GeV state in each phase in terms of its couplings to SM particles and its signal strengths at collider experiments normalised to the respective SM values. We observed that the squared couplings of the h_{125} in the IDP to both vector bosons and fermions are modified compared to the SM with one common factor in the range 0.78 up to unity. This is reflected directly in the signal strengths. Only in the $\gamma\gamma$ channel, the IDP allows for significantly enhanced signal strengths compared to the SM. On the contrary, the DSP allows for considerably more room for deviations from the SM in terms of diminished as well as enhanced signal strengths in all but the photonic decay channel. We conclude that more precise measurements, especially in the photonic and fermionic decay channels, would allow to constrain the parameter space of the two phases. We further investigated how to distinguish between the two phases assuming that one additional Higgs boson is discovered at collider experiments. The DSP is compatible with the discovery of a charged or a neutral Higgs boson, whereas the IDP would be ruled out by the discovery of a charged state, because the

charged Higgs boson is DM. Nor could the IDP explain the discovery of a neutral CP-odd Higgs boson, while the DSP could. However, both phases allow for an additional neutral CP-even state to be discovered. We observed that the DSP only allows for masses of the additional Higgs boson of up to 700 GeV. Therefore, the discovery of a heavier Higgs boson would rule out this phase. In order to further examine which kind of observations could or could not be explained by the IDP or DSP, we investigated the inclusive production and decay rates for decays into a pair of SM particles. The ZZ decay channel does not allow to discriminate between the two phases. In the channels $\tau\bar{\tau}$ and $\gamma\gamma$, on the contrary, the discovery of a Higgs boson with a mass above 200 GeV could be easily explained only by the DSP. In the IDP, the inclusive cross sections are too small in order to be measurable at the LHC. The discovery of a Higgs boson with a mass below 63 GeV in the $\tau\bar{\tau}$ channels could be explained by the IDP but would put the DSP under strain. Otherwise, it is difficult to distinguish between the two phases solely on the basis of inclusive cross sections.

In addition, we studied the properties of the dark sector and the impact of DM constraints on both the visible and dark sector of each phase. In the visible sector, we compared the distribution of points compatible with direct detection constraints to those of the whole sample. However, the statistics are too low to establish definitively whether there is an impact on the visible sector or not. Regarding the dark sector of the IDP, we found that the charged dark state is ruled out as lightest dark particle due to direct detection constraints. Furthermore, we showed that the IDP by itself is not sufficient to explain the observed DM relic abundance. The DSP, in contrary, allows for DM candidates with masses above 200 GeV that can provide the observed relic abundance.

Future work should aim at increasing the statistics in order to further investigate the impact of DM direct detection constraints on the visible and dark sectors of each phase. Furthermore, it would be interesting to study the different behaviour of the IDP and the DSP in terms of the inclusive production and decay cross section of the second visible CP-even Higgs boson in the $\tau\bar{\tau}$ channel at masses below 63 GeV. Besides, it would be worth considering the two phases in the light of new constraints through the upcoming `HiggsBounds 5`, especially regarding invisible decays such as $X_D^i \rightarrow X_D^j + Z/W^\pm$ in the IDP.

A. Appendix: Inert Doublet Phase

In this chapter, we give further information on the IDP. In Section A.1, we present the formulae for the transformation from the Lagrangian to the physical parameter set. In Section A.2, we provide formulae for the triple-Higgs couplings.

A.1. Explicit Parameter Transformations

In this section, we derive the formulae that allow to convert from the Lagrangian parameter set of Eq. (3.7) to the physical parameter set of Eq. (3.8). First, we use the stationary conditions for the VEVs (see Eqs. (2.8a)-(2.8c)) in order to trade two of the mass parameters of the Lagrangian for the VEVs as follows

$$m_{22}^2 \stackrel{(2.8b)}{=} -\frac{1}{2} (v^2 \lambda_2 + v_s^2 \lambda_8), \quad (\text{A.1a})$$

$$m_S^2 \stackrel{(2.8c)}{=} -\frac{1}{2} (v_s^2 \lambda_6 + v^2 \lambda_8). \quad (\text{A.1b})$$

For the diagonalisation of the neutral CP-even sector, we use the mixing matrix given in Eq. (3.2). This yields the following relations between the masses of the neutral CP-even Higgs bosons and a subset of Lagrangian parameters:

$$m_{H_1}^2 = v^2 \cos^2 \alpha \lambda_2 + v_s^2 \sin^2 \alpha \lambda_6 + 2vv_s \sin \alpha \cos \alpha \lambda_8, \quad (\text{A.2a})$$

$$m_{H_2}^2 = v^2 \sin^2 \alpha \lambda_2 + v_s^2 \cos^2 \alpha \lambda_6 - 2vv_s \sin \alpha \cos \alpha \lambda_8, \quad (\text{A.2b})$$

$$m_{H_D}^2 = \frac{1}{2} (2m_{11}^2 + v^2 (\lambda_3 + \lambda_4 + \lambda_5) + v_s^2 \lambda_7). \quad (\text{A.2c})$$

We further use the mixing matrix

$$\mathcal{U} \stackrel{(3.4)}{=} \begin{pmatrix} 0 & 1 \\ -1 & 0 \end{pmatrix}, \quad (\text{A.3})$$

to diagonalise the charged and neutral CP-odd sectors, which yields

$$m_{A_D}^2 = \frac{1}{2} (2m_{11}^2 + v^2 (\lambda_3 + \lambda_4 - \lambda_5) + v_s^2 \lambda_7), \quad (\text{A.4a})$$

$$m_{H_D^\pm}^2 = \frac{1}{2} (2m_{11}^2 + v^2 \lambda_3 + v_s^2 \lambda_7). \quad (\text{A.4b})$$

Equations (A.2a)-(A.2c), (A.4a)-(A.4b) and the requirement for the neutral CP-even mass matrix to be diagonal allow to express six of the dimensionless parameters of the Lagrangian in terms of the physical masses, the mixing angle α and the VEVs v and v_s as follows

$$\lambda_2 = \frac{1}{v^2} \left(\sum_i m_{H_i}^2 \cdot \mathcal{R}_{i2}^2 \right), \quad (\text{A.5a})$$

$$\lambda_3 = \frac{1}{v^2} \left(2 \left(m_{H_D^\pm}^2 - m_{11}^2 \right) - v_s^2 \lambda_7 \right), \quad (\text{A.5b})$$

$$\lambda_4 = \frac{1}{v^2} \left(m_{A_D}^2 + m_{H_D}^2 - 2 \cdot m_{H^\pm}^2 \right), \quad (\text{A.5c})$$

$$\lambda_5 = \frac{1}{v^2} \left(m_{H_D}^2 - m_{A_D}^2 \right), \quad (\text{A.5d})$$

$$\lambda_6 = \frac{1}{v_s^2} \left(\sum_i m_{H_i}^2 \cdot \mathcal{R}_{i3}^2 \right), \quad (\text{A.5e})$$

$$\lambda_8 = \frac{1}{v v_s} \left(\sum_i m_{H_i}^2 \cdot \mathcal{R}_{i2} \cdot \mathcal{R}_{i3} \right), \quad (\text{A.5f})$$

where \mathcal{R}_{ij} is the i, j element of the mixing matrix in Eq. (3.2). The parameters m_{11}^2 , λ_1 and λ_7 cannot be expressed through physical parameters and thus remain independent parameters in the physical parameter set of the IDP.

A.2. Triple-Higgs Couplings

In this section we give the formulae for the triple-Higgs couplings $g(X_i X_j X_k)$ in the IDP. A coupling $g(X_i X_j X_k)$ is defined as

$$g(X_i X_j X_k) = \frac{\partial^3 \mathcal{L}}{\partial X_i \partial X_j \partial X_k}, \quad (\text{A.6})$$

with $X_{i/j/k} \in \{H_1, H_2, H_D, A_D, H_D^\pm\}$. In the following, the indices i, j can take unique values of $\{1, 2\}$ and denote one of the visible CP-even Higgs bosons H_1 or H_2 , respectively. All couplings with an odd number of dark Higgs bosons vanish due to the conserved dark parity. The non-zero triple-Higgs couplings are the following:

$$g(H_i H_i H_i) = + 3 \lambda_2 v \cdot \mathcal{R}_{i2}^3 + 3 \lambda_6 v_s \cdot \mathcal{R}_{i3}^3 + 3 \lambda_8 (v \mathcal{R}_{i2} \cdot \mathcal{R}_{i3}^2 + v_s \cdot \mathcal{R}_{i3} \cdot \mathcal{R}_{i2}^2), \quad (\text{A.7})$$

$$g(H_i H_j H_j) = + 3 \lambda_2 v \cdot \mathcal{R}_{i2} \cdot \mathcal{R}_{j2}^2 + 3 \lambda_6 v_s \cdot \mathcal{R}_{i3} \cdot \mathcal{R}_{j3}^2 + \lambda_8 [v \cdot (\mathcal{R}_{i2} \cdot \mathcal{R}_{j3}^2 + 2 \mathcal{R}_{i3} \cdot \mathcal{R}_{j2} \cdot \mathcal{R}_{j3}) + v_s \cdot (\mathcal{R}_{i3} \cdot \mathcal{R}_{j2}^2 + 2 \mathcal{R}_{i2} \cdot \mathcal{R}_{j2} \cdot \mathcal{R}_{j3})], \quad (\text{A.8})$$

$$g(H_i H_D H_D) = \frac{2}{v} (m_{H_D}^2 - m_{11}^2) \mathcal{R}_{i2} + \lambda_7 \frac{v_s}{v} (v \cdot \mathcal{R}_{i3} - v_s \cdot \mathcal{R}_{i2}), \quad (\text{A.9})$$

$$g(H_i H_D^\pm H_D^-) = \frac{2}{v} (m_{H_D^\pm}^2 - m_{11}^2) \mathcal{R}_{i2} + \lambda_7 \frac{v_s}{v} (v \cdot \mathcal{R}_{i3} - v_s \cdot \mathcal{R}_{i2}), \quad (\text{A.10})$$

$$g(H_i A_D A_D) = \frac{2}{v} (m_{A_D}^2 - m_{11}^2) \mathcal{R}_{i2} + \lambda_7 \frac{v_s}{v} (v \cdot \mathcal{R}_{i3} - v_s \cdot \mathcal{R}_{i2}). \quad (\text{A.11})$$

B. Appendix: Dark Singlet Phase

In this chapter, we give further information on the DSP. In Section B.1, we present the formulae for the transformation from the Lagrangian to the physical parameter set. In Section B.2, we provide formulae for the triple-Higgs couplings. In the following, we consider the softly- \mathbb{Z}_2 -broken potential. For generality, all formulae for the \mathbb{Z}_2 -conserving potential can easily be determined by setting $m_{12}^2 = 0$.

B.1. Explicit Parameter Transformations

In this section, we derive the formulae that allow to convert from the Lagrangian parameter set of Eq. (3.18) to the physical parameter set of Eq. (3.19). First, we use the stationary conditions for the VEVs (see Eqs (2.8a)-(2.8c)) in order to trade two of the mass parameters of the Lagrangian for the VEVs as follows

$$m_{11}^2 - \frac{v_2}{v_1} m_{12}^2 \stackrel{(2.8a)}{=} -\frac{1}{2} (v_1^2 \lambda_1 + v_2^2 \lambda_{345}), \quad (\text{B.1a})$$

$$m_{22}^2 - \frac{v_1}{v_2} m_{12}^2 \stackrel{(2.8b)}{=} -\frac{1}{2} (v_1^2 \lambda_{345} + v_2^2 \lambda_2). \quad (\text{B.1b})$$

For the diagonalisation of the neutral CP-even sector, we use the mixing matrix given in Eq. (3.14). This yields the following relations between the masses of the neutral CP-even Higgs bosons and a subset of Lagrangian parameters:

$$m_{H_1}^2 = \frac{m_{12}^2}{v_1 v_2} (v_1 \cos \alpha + v_2 \sin \alpha)^2 + \lambda_1 v_1^2 \cos^2 \alpha + \lambda_2 v_2^2 \sin^2 \alpha - 2\lambda_{345} v_1 v_2 \cos \alpha \sin \alpha, \quad (\text{B.2a})$$

$$m_{H_2}^2 = + \frac{m_{12}^2}{v_1 v_2} (v_1 \sin \alpha - v_2 \cos \alpha)^2 + \lambda_1 v_1^2 \cos^2 \alpha + \lambda_2 v_2^2 \sin^2 \alpha + 2\lambda_{345} v_1 v_2 \cos \alpha \sin \alpha, \quad (\text{B.2b})$$

$$m_{H_D}^2 = \frac{1}{2} (2m_s^2 + v_1^2 \lambda_7 + v_2^2 \lambda_8). \quad (\text{B.2c})$$

We further use the mixing matrix in Eq. (3.4) to diagonalise the charged and neutral CP-odd sectors, which yields

$$m_A^2 = -v^2 \lambda_5 + \frac{m_{12}^2}{s_\beta c_\beta}, \quad (\text{B.3a})$$

$$m_{H^\pm}^2 = -\frac{1}{2} v^2 (\lambda_4 + \lambda_5) + \frac{m_{12}^2}{s_\beta c_\beta}. \quad (\text{B.3b})$$

Equations (B.2a)-(B.2c), (B.3a)-(B.3b) and the requirement for the neutral CP-even mass matrix to be diagonal allow to express six of the dimensionless parameters of the Lagrangian in terms of the physical masses, the mixing angle α , the VEV v and $\tan\beta$ as follows

$$m_S^2 = -\frac{1}{2} (v_1^2 \lambda_7 + v_2^2 \lambda_8 - 2m_{H_D}), \quad (\text{B.4a})$$

$$\lambda_1 = \frac{1}{v^2 c_\beta^2} \left[\left(\sum_i m_{H_i}^2 \cdot \mathcal{R}_{i1}^2 \right) - m_{12}^2 \frac{s_\beta}{c_\beta} \right], \quad (\text{B.4b})$$

$$\lambda_2 = \frac{1}{v^2 s_\beta^2} \left[\left(\sum_i m_{H_i}^2 \cdot \mathcal{R}_{i2}^2 \right) - m_{12}^2 \frac{c_\beta}{s_\beta} \right], \quad (\text{B.4c})$$

$$\lambda_3 = \frac{1}{v^2 c_\beta s_\beta} \left[\left(\sum_i m_{H_i}^2 \cdot \mathcal{R}_{i1} \mathcal{R}_{i2} \right) - m_{12}^2 \right] + \frac{2}{v^2} m_{H^\pm}^2, \quad (\text{B.4d})$$

$$\lambda_4 = \frac{1}{v^2} (m_A^2 - 2m_{H^\pm}^2) + \frac{1}{v^2 c_\beta s_\beta} m_{12}^2, \quad (\text{B.4e})$$

$$\lambda_5 = -\frac{1}{v^2} m_A^2 + \frac{1}{v^2 c_\beta s_\beta} m_{12}^2. \quad (\text{B.4f})$$

where \mathcal{R}_{ij} is the i, j element of the mixing matrix in Eq. (3.14). The parameters λ_6 , λ_7 and λ_8 cannot be expressed through physical parameters and thus remain independent parameters in the physical parameter set of the DSP.

B.2. Triple-Higgs Couplings

In this section we give the formulae for the triple-Higgs couplings $g(X_i X_j X_k)$ in the DSP. The definition of the coupling $g(X_i X_j X_k)$ is given in Eq. (A.6) with $X_{i/j/k} \in \{H_1, H_2, H_D, A, H^\pm\}$. In the following, the indices i, j can take unique values of $\{1, 2\}$ and denote one of the visible CP-even Higgs bosons H_1 or H_2 , respectively. All couplings with an odd number of H_D vanish due to the conserved dark parity. The non-zero triple-Higgs couplings are the following:

$$g(H_i H_i H_i) = 3v [c_\beta (\mathcal{R}_{i1}^3 \lambda_1 + \mathcal{R}_{i1} \mathcal{R}_{i2}^2 \lambda_{345}) + s_\beta (\mathcal{R}_{i2}^3 \lambda_2 + \mathcal{R}_{i2} \mathcal{R}_{i1}^2 \lambda_{345})], \quad (\text{B.5})$$

$$g(H_i H_j H_j) = v \left[c_\beta (3\mathcal{R}_{i1} \mathcal{R}_{j1}^2 \lambda_1 + (3\mathcal{R}_{i2} \mathcal{R}_{j1} \mathcal{R}_{j2} + \mathcal{R}_{i1}) \lambda_{345}) \right. \\ \left. + v s_\beta (3\mathcal{R}_{i2} \mathcal{R}_{j2}^2 \lambda_2 + (3\mathcal{R}_{i1} \mathcal{R}_{j1} \mathcal{R}_{j2} + \mathcal{R}_{i2}) \lambda_{345}) \right], \quad (\text{B.6})$$

$$g(H_i A A) = v \left[c_\beta (c_\beta s_\beta \mathcal{R}_{i2} (\lambda_2 - 2\lambda_5) + c_\beta^2 \mathcal{R}_{i1} \lambda_{34-5}) \right. \\ \left. + s_\beta (c_\beta s_\beta \mathcal{R}_{i2} (\lambda_1 - 2\lambda_5) + s_\beta^2 \mathcal{R}_{i2} \lambda_{34-5}) \right], \quad (\text{B.7})$$

$$g(H_i H^+ H^-) = v \left[c_\beta (s_\beta^2 \mathcal{R}_{i1} \lambda_1 + c_\beta^2 \mathcal{R}_{i1} \lambda_3 - c_\beta s_\beta \mathcal{R}_{i2} (\lambda_4 + \lambda_5)) \right. \\ \left. + s_\beta (c_\beta^2 \mathcal{R}_{i2} \lambda_2 + s_\beta^2 \mathcal{R}_{i2} \lambda_3 - c_\beta s_\beta \mathcal{R}_{i1} (\lambda_4 + \lambda_5)) \right], \quad (\text{B.8})$$

$$g(H_i H_D H_D) = v [c_\beta \mathcal{R}_{i,1} \lambda_7 + s_\beta \mathcal{R}_{i,2} \lambda_8]. \quad (\text{B.9})$$

C. Global Minimum Conditions for the \mathbb{Z}_2 -Conserving Potential

In this chapter, we present the conditions for a stationary point of the \mathbb{Z}_2 -conserving potential to be a global minimum of the potential. First, we identify all possible solutions of the stationary conditions for the C- and CP-conserving VEVs v_1 , v_2 and v_s as well as the charge-breaking VEV v_{cb} and the CP-breaking VEV v_{cp} , as described in Section 4.1.2. In Sections C.1 and C.2, we derive the value of the scalar potential for each of the cases listed in Tables 4.2 and 4.3, respectively. The special cases, i.e. the cases that only exist for specific choices of Lagrangian parameters listed in Table 4.1, are considered separately in Section C.3. The definition of the most general static field configuration, see Eq. (4.6), is such that the VEVs are real parameters. Therefore, we state the positivity conditions for the squared VEVs, which are the conditions for the solution to satisfy this requirement, together with the corresponding stationary values of the scalar potential. In order to shorten the expressions, we introduce the following short-hand term:

$$\Lambda_{kl}^{ij} = \lambda_i \lambda_j - \lambda_k \lambda_l. \quad (\text{C.1})$$

We summarise our findings in Section C.4.

C.1. 2HDM-Like Stationary Points

In this section, we derive the stationary values and positivity conditions for the cases with $v_s = 0$, see Table 4.2.

C.1.1. Case I

We consider $v_1, v_2 \neq 0$ while $v_{\text{cb}} = v_{\text{cp}} = 0$. The stationary value of this CP- and charge-conserving case is

$$V(\text{I}) = \frac{(m_{11}^2)^2 \lambda_2 + (m_{22}^2)^2 \lambda_1 - 2m_{11}^2 m_{22}^2 x}{2\Lambda_{12}^{xx}}, \quad (\text{C.2})$$

with $x = \lambda_3 + \lambda_4 + \lambda_5$. The conditions for this solution to exist are

$$0 < v_1^2 = \frac{2(m_{11}^2 \lambda_2 - m_{22}^2 x)}{\Lambda_{12}^{xx}}, \quad (\text{C.3a})$$

$$0 < v_2^2 = \frac{2(-m_{11}^2 x + m_{22}^2 \lambda_1)}{\Lambda_{12}^{xx}}. \quad (\text{C.3b})$$

C.1.2. Case III

Case III considers $v_1 = v_2 = 0$ involving three sub-cases with either

$$v_{cb} \neq 0, \quad v_{cp} \neq 0, \quad (\text{C.4a})$$

$$v_{cp} \neq 0, \quad v_{cb} = 0, \quad (\text{C.4b})$$

$$v_{cb} = 0, \quad v_{cp} \neq 0. \quad (\text{C.4c})$$

All three CP- and /or charge-breaking cases lead to the same stationary value

$$V(\text{IIIabc}) = -\frac{(m_{22}^2)^2}{2\lambda_2}. \quad (\text{C.5})$$

Simplifying the positivity conditions of the squared VEVs results in:

$$0 < -\frac{2m_{22}^2}{\lambda_2}. \quad (\text{C.6})$$

Since the conditions for the potential to be bounded from below (see Section 4.1.1) requires $\lambda_2 > 0$, $m_{22}^2 < 0$ is required for the solution to exist.

C.1.3. Case IV

Case IV includes all cases with $v_1 \neq 0$, $v_2 = 0$ and different combinations of zero and non-zero v_{cb} and v_{cp} . For the case IVa, where $v_{cb} = v_{cp} = 0$, the positivity condition is

$$0 < v_1^2 = -\frac{2m_{11}^2}{\lambda_1}. \quad (\text{C.7})$$

In combination with $\lambda_1 > 0$, which results from the conditions for the potential to be bounded from below, this implies $m_{11}^2 < 0$. The stationary value of the scalar potential for case IVa is given by

$$V(\text{IVa}) = -\frac{(m_{11}^2)^2}{2\lambda_1}. \quad (\text{C.8})$$

The cases IVc ($v_{cp} \neq 0$) and IVd ($v_{cb} \neq 0$) only exist if

$$0 < v_1^2 = \frac{2(-m_{11}^2\lambda_2 + m_{22}^2x)}{\Lambda_{xx}^{12}}, \quad (\text{C.9a})$$

$$0 < v_i^2 = \frac{2(m_{11}^2x - m_{22}^2\lambda_1)}{\Lambda_{xx}^{12}} \quad (\text{C.9b})$$

are fulfilled, where $v_i = v_{cp}$ for the case IVc and $v_i = v_{cb}$ for the case IVd. The short-hand term x denotes

$$x = \begin{cases} \lambda_{34-5} & (\text{IVc}), \\ \lambda_3 & (\text{IVd}). \end{cases} \quad (\text{C.10})$$

The corresponding stationary value of the scalar potential is

$$V(\text{IVc/d}) = \frac{(m_{11}^2)^2\lambda_2 + (m_{22}^2)^2\lambda_1 - 2m_{11}^2m_{22}^2x}{2\Lambda_{xx}^{12}}. \quad (\text{C.11})$$

C.1.4. Case V

Case V covers all sub-cases with $v_1 = 0$, $v_2 \neq 0$ and different combinations of zero and non-zero v_{cb} and v_{cp} . The positivity conditions of all four cases yield

$$0 < -\frac{2m_{22}^2}{\lambda_2}. \quad (\text{C.12})$$

Analogously to case III, the cases Va-d are only solutions of the stationary conditions if $m_{22}^2 < 0$. All four sub-cases lead to the same stationary value

$$V(\text{Vabcd}) = -\frac{(m_{22}^2)^2}{2\lambda_2}. \quad (\text{C.13})$$

C.2. Stationary Points With a Non-Zero Singlet Vacuum Expectation Value

In this section, we derive the stationary values and positivity conditions for the cases with $v_s \neq 0$, see Table 4.3.

C.2.1. Case sI

Analogously to case I, case sI covers the CP- and charge-conserving case with $v_1, v_2 \neq 0$ and non-vanishing singlet VEV. In order for cases I to exist, the positivity conditions

$$0 < v_1^2 = \frac{2(m_{11}^2 \Lambda_{26}^{88} - m_{22}^2 \Lambda_{x6}^{78} - m_s^2 \Lambda_{27}^{x8})}{x \Lambda_{x6}^{78} + \lambda_7 \Lambda_{27}^{x8} - \lambda_1 \Lambda_{26}^{88}}, \quad (\text{C.14a})$$

$$0 < v_2^2 = \frac{2(-m_{11}^2 \Lambda_{x6}^{78} + m_{22}^2 \Lambda_{16}^{77} - m_s^2 \Lambda_{18}^{x7})}{x \Lambda_{x6}^{78} + \lambda_7 \Lambda_{27}^{x8} - \lambda_1 \Lambda_{26}^{88}}, \quad (\text{C.14b})$$

$$0 < v_s^2 = \frac{2(-m_{11}^2 \Lambda_{27}^{x8} - m_{22}^2 \Lambda_{18}^{x7} + m_s^2 \Lambda_{12}^{xx})}{x \Lambda_{x6}^{78} + \lambda_7 \Lambda_{27}^{x8} - \lambda_1 \Lambda_{26}^{88}}, \quad (\text{C.14c})$$

where x denotes $\lambda_3 + \lambda_4 + \lambda_5$, must be fulfilled. The corresponding stationary value of the scalar potential is given by

$$V(\text{sI}) = \frac{(m_{11}^2)^2 \Lambda_{26}^{88} + (m_{22}^2)^2 \Lambda_{16}^{77} + (m_s^2)^2 \Lambda_{12}^{xx}}{2(-\lambda_1 \Lambda_{26}^{88} + x \Lambda_{x6}^{78} + \lambda_7 \Lambda_{27}^{x8})} - \frac{m_{11}^2 m_{22}^2 \Lambda_{x6}^{78} + m_s^2 (m_{11}^2 \Lambda_{27}^{x8} + m_{22}^2 \Lambda_{18}^{x7})}{x \Lambda_{x6}^{78} + \lambda_7 \Lambda_{27}^{x8} - \lambda_1 \Lambda_{26}^{88}}. \quad (\text{C.15})$$

C.2.2. Case sIII

Case sIII is the analogy to case III with $v_s \neq 0$, i.e. we have $v_1 = v_2 = 0$ with the three sub-cases

$$v_{cb} \neq 0, \quad v_{cp} \neq 0, \quad (\text{C.16a})$$

$$v_{cp} \neq 0, \quad v_{cb} = 0, \quad (\text{C.16b})$$

$$v_{cb} = 0, \quad v_{cp} \neq 0. \quad (\text{C.16c})$$

Each of the three sub-cases results in the following positivity conditions

$$0 < v_{cp}^2 + v_{cb}^2 = \frac{2(m_{22}^2 \lambda_6 - m_s^2 \lambda_8)}{\Lambda_{26}^{88}}, \quad (\text{C.17a})$$

$$0 < v_s^2 = \frac{2(-m_{22}^2 \lambda_8 + m_s^2 \lambda_2)}{\Lambda_{26}^{88}}. \quad (\text{C.17b})$$

The stationary value of the scalar potential corresponding to all three cases reads

$$V(\text{sIIIabc}) = \frac{(m_{22}^2)^2 \lambda_6 + (m_s^2)^2 \lambda_2 - 2m_{22}^2 m_s^2 \lambda_8}{2\Lambda_{26}^{88}}. \quad (\text{C.18})$$

C.2.3. Case sIV

Case sIVa, where only v_1 and v_s do not vanish, exists when fulfilling the following positivity conditions

$$0 < v_1^2 = \frac{2(m_{11}^2 \lambda_6 - m_s^2 \lambda_7)}{\Lambda_{16}^{77}}, \quad (\text{C.19a})$$

$$0 < v_s^2 = \frac{2(-m_{11}^2 \lambda_7 + m_s^2 \lambda_1)}{\Lambda_{16}^{77}}. \quad (\text{C.19b})$$

Furthermore, it yields the following stationary value of the scalar potential

$$V(\text{sIVa}) = \frac{(m_{11}^2)^2 \lambda_6 + (m_s^2)^2 \lambda_1 - m_{11}^2 m_s^2 \lambda_7}{2\Lambda_{16}^{77}}. \quad (\text{C.20})$$

In the cases sIVc and sIVd, where additionally to $v_1 \neq 0$ and $v_s \neq 0$ also $v_{\text{cp}} \neq 0$ or $v_{\text{cb}} \neq 0$, respectively, the positivity conditions are

$$0 < v_1^2 = \frac{2(m_{11}^2 \Lambda_{26}^{88} - m_{22}^2 \Lambda_{x6}^{78} - m_s^2 \Lambda_{27}^{x8})}{x\Lambda_{x6}^{78} + \lambda_7 \Lambda_{27}^{x8} - \lambda_1 \Lambda_{26}^{88}}, \quad (\text{C.21a})$$

$$0 < v_s^2 = \frac{2(m_{11}^2 \Lambda_{x8}^{27} + m_{22}^2 \Lambda_{x7}^{18} + m_s^2 \Lambda_{12}^{xx})}{x\Lambda_{x6}^{78} + \lambda_7 \Lambda_{27}^{x8} - \lambda_1 \Lambda_{26}^{88}}, \quad (\text{C.21b})$$

$$0 < v_i^2 = -\frac{2(m_{11}^2 \Lambda_{x6}^{78} - m_{22}^2 \Lambda_{16}^{77} + m_s^2 \Lambda_{18}^{x7})}{x\Lambda_{x6}^{78} + \lambda_7 \Lambda_{27}^{x8} - \lambda_1 \Lambda_{26}^{88}}, \quad (\text{C.21c})$$

where

$$x = \begin{cases} \lambda_{34-5} & (\text{sIVc}), \\ \lambda_3 & (\text{sIVd}). \end{cases} \quad (\text{C.22})$$

The corresponding stationary value of the scalar potential is

$$V(\text{sIVcd}) = \frac{(m_{11}^2)^2 \Lambda_{26}^{88} + (m_{22}^2)^2 \Lambda_{16}^{77} + (m_s^2)^2 \Lambda_{12}^{xx}}{2(x\Lambda_{x6}^{78} + \lambda_7 \Lambda_{27}^{x8} - \lambda_1 \Lambda_{26}^{88})} + \frac{m_{11}^2 m_{22}^2 \Lambda_{x6}^{x6} + m_s^2 (m_{22}^2 \Lambda_{x7}^{18} + m_{11}^2 \Lambda_{x8}^{27})}{x\Lambda_{x6}^{78} + \lambda_7 \Lambda_{27}^{x8} - \lambda_1 \Lambda_{26}^{88}}. \quad (\text{C.23})$$

C.2.4. Case sV

Case sV covers the sub-cases with $v_1 = 0$, $v_2 \neq 0$, $v_s \neq 0$ and different combinations of zero or non-zero v_{cp} and v_{cb} . In order to be a valid solution of the stationary conditions, each of these cases has to fulfil the following positivity conditions

$$0 < v_2^2 + v_{\text{cp}}^2 + v_{\text{cb}}^2 = \frac{2(m_{22}^2 \lambda_6 - m_s^2 \lambda_8)}{\Lambda_{26}^{88}}, \quad (\text{C.24a})$$

$$0 < v_s^2 = \frac{-2(m_{22}^2 \lambda_8 - m_s^2 \lambda_2)}{\Lambda_{26}^{88}}. \quad (\text{C.24b})$$

The stationary value of the potential corresponding to sVa-d reads

$$V(\text{sVabcd}) = \frac{(m_s^2)^2 \lambda_2 + (m_{22}^2)^2 \lambda_6 - m_{22}^2 m_s^2 \lambda_8}{2\Lambda_{26}^{88}}. \quad (\text{C.25})$$

Table C.1.: VEV configurations for the solutions (C.30)-(C.31c) of the special cases $\lambda_5 = 0$, $\lambda_5 = -\lambda_4$ and $\lambda_5 = \lambda_4$.

Case	v_i	v_j	Condition
IIa	v_2	v_{cp}	$\lambda_5 = 0$
IIb	v_2	v_{cb}	$\lambda_5 = -\lambda_4$
IVb	v_{cp}	v_{cb}	$\lambda_5 = \lambda_4$

C.2.5. Case s

The case s describes the situation where all VEVs are zero, except for v_s . The condition for this case to be a solution of the stationary conditions is

$$0 < v_s^2 = -\frac{2m_s^2}{\lambda_6}. \quad (\text{C.26})$$

Since λ_6 is required to be positive due to boundedness from below, this case only exists for $m_s^2 < 0$. The corresponding stationary value of the potential is

$$V(s) = -\frac{(m_s^2)^2}{2\lambda_6}. \quad (\text{C.27})$$

C.3. Special Cases

For particular choices of Lagrangian parameters, additional cases become possible. In this section, we derive the stationary values of the potential and the positivity conditions for the cases listed in Table 4.1.

Regarding the cases with vanishing singlet VEV, choosing λ_5 to be zero, allows for case IIa, where $v_1, v_2, v_{\text{cp}} \neq 0$. Choosing $\lambda_5 = -\lambda_4$ allows for v_1, v_2 and v_{cp} to be simultaneously non-zero (case IIb). If $\lambda_5 = \lambda_4$, case IVb is allowed, i.e. the case of v_1, v_{cp} and v_{cb} being simultaneously non-zero. All three cases are covered with the following positivity conditions

$$0 < v_i^2 + v_j^2 = -\frac{2m_{11}^2 x - 2m_{22}^2 \lambda_1}{\Lambda_{12}^{xx}}, \quad (\text{C.28a})$$

$$0 < v_1^2 = -\frac{-2m_{11}^2 \lambda_2 + 2m_{22}^2 x}{\Lambda_{12}^{xx}}, \quad (\text{C.28b})$$

where v_i and v_j are chosen according to table C.1. x is introduced as a short-hand term for

$$x = \begin{cases} \lambda_3 + \lambda_4 & (\text{IIa}), \\ \lambda_3 & (\text{IIb and IVb}). \end{cases} \quad (\text{C.29})$$

The three configurations yield a scalar-potential value of

$$V(\text{II}) = \frac{(m_{11}^2)^2 \lambda_2 - 2m_{11}^2 m_{22}^2 x + (m_{22}^2)^2 \lambda_1}{2\Lambda_{12}^{xx}}. \quad (\text{C.30})$$

Considering a non-zero singlet VEV implies the following positivity conditions

$$0 < v_i^2 + v_j^2 = \frac{2(m_{11}^2 \Lambda_{78}^{x6} + m_{22}^2 \Lambda_{16}^{77} + m_s^2 \Lambda_{x7}^{18})}{(\lambda_7 \Lambda_{27}^{x8} + x \Lambda_{x6}^{78} - \lambda_1 \Lambda_{26}^{88})}, \quad (\text{C.31a})$$

$$0 < v_1^2 = \frac{2(m_{11}^2 \Lambda_{26}^{88} + m_{22}^2 \Lambda_{78}^{x6} + m_s^2 \Lambda_{x8}^{27})}{(\lambda_7 \Lambda_{27}^{x8} + x \Lambda_{x6}^{78} - \lambda_1 \Lambda_{26}^{88})}, \quad (\text{C.31b})$$

$$0 < v_s^2 = \frac{2(m_s^2 \Lambda_{12}^{xx} + m_{11}^2 \Lambda_{x8}^{27} + m_{22}^2 \Lambda_{x7}^{18})}{(\lambda_7 \Lambda_{27}^{x8} + x \Lambda_{x6}^{78} - \lambda_1 \Lambda_{26}^{88})}, \quad (\text{C.31c})$$

with x analogously to the cases IIa, IIb and IVb (see Eq. (C.29)). The corresponding stationary value of the scalar potential reads

$$V(\text{II}) = \frac{(m_{11}^2)^2 \Lambda_{26}^{88} + (m_{22}^2)^2 \Lambda_{16}^{77} + (m_s^2)^2 \Lambda_{12}^{xx}}{2(\lambda_7 \Lambda_{27}^{x8} + x \Lambda_{x6}^{78} - \lambda_1 \Lambda_{26}^{88})} \quad (\text{C.32})$$

$$- \frac{m_{11}^2 m_{22}^2 \Lambda_{x6}^{78} + m_s^2 (m_{11}^2 \Lambda_{27}^{x8} + m_{22}^2 \Lambda_{18}^{x7})}{\lambda_7 \Lambda_{27}^{x8} + x \Lambda_{x6}^{78} - \lambda_1 \Lambda_{26}^{88}}. \quad (\text{C.33})$$

C.4. Summary

We observe that certain cases share the same positivity conditions and potential values. The results of case V equal those of case III. Likewise, the results of case sV equal those of case sIII. We further note that the cases (s)IVc and (s)IVd extend case (s)I, because they only differ in the variable x as follows

$$x = \begin{cases} \lambda_3 + \lambda_4 + \lambda_5 & (\text{I}), \\ \lambda_3 + \lambda_4 - \lambda_5 & (\text{IVc}), \\ \lambda_3 & (\text{IVd}). \end{cases} \quad (\text{C.34})$$

The special cases (s)IIb and (s)IVb yield the same results as the case (s)IVd and special case (s)IIa equals to the cases (s)I and (s)IVc, because $\lambda_{345} = \lambda_{34-5}$ for $\lambda_5 = 0$. Therefore, these cases do not further constrain the parameter space. In conclusion, there are five 2HDM-like cases (I, III, IVa, IVc and IVd) and six cases with non-vanishing singlet VEV (sI, sIII, sIVa, sIVc, sIVd and s) that differ in their results and need to be considered separately in order to determine whether the physical vacuum of the potential is the global one.

Acknowledgements

First of all, I would like to thank Prof. Dr. Margarete Mühlleitner for the interesting topic of this work and the opportunity to join her working group. I am especially grateful for the continuous support and the great atmosphere throughout the year. Many thanks also for organising the research trip to Lisbon which was a wonderful experience.

I would like to express my gratitude to Prof. Dr. Thomas Schwetz-Mangold, who agreed to be the second reviewer of this work.

My sincere thanks go to Jonas Wittbrodt, who acted as remote advisor. I would like to thank him for countless things, but in particular for sharing his knowledge about `N2HDECAY` and `ScannerS`, for answering almost every question I had and, of course, for all the fun during work.

Special thanks to Prof. Dr. Rui Santos for his hospitality during our stay in Lisbon and for his excellent suggestion to compare the inert doublet phase to another DM model.

In addition, I would like to thank Marcel Krause for his help during my introductory period, Philipp Basler and Jonas Müller for all the interesting discussions about the N2HDM, and Dr. Florian Staub for providing and explaining to me `SARAH`, which has facilitated many things.

Thanks to all members of the Institute of Theoretical Physics for the company over lunch or coffee, the interesting discussions on a variety of topics, the tasty cakes and the overall wonderful time.

Last but not least, I would like to thank my family and friends for their support, but also for the distraction in stressful times.

Glossary

- 2HDM** Two-Higgs-Doublet Model. 2, 4, 5, 8–10, 28, 39
- bbH** Higgs production via b -quark fusion. 15, 20, 26, 27, 31
- BSM** Physics beyond the Standard Model. 1, 15, 28, 33
- DM** Dark matter. 1, 2, 4, 7, 9–11, 16, 17, 20, 21, 23, 28, 34–40
- DSP** Dark singlet phase of the Next-to-Two-Higgs-Doublet Model. 2, 7, 9–11, 15, 19–21, 23–25, 27, 28, 30–40, 43, 44
- EWSB** Electroweak symmetry breaking. 1, 2, 4, 7, 39
- FCNC** Flavour-changing neutral currents. 5, 9
- ggH** Higgs production via gluon fusion. 15, 20, 26, 27, 31, 32
- IDM** Inert Two-Higgs-Doublet Model. 1, 30
- IDP** Inert doublet phase of the Next-to-Two-Higgs-Doublet Model. 2, 4, 7, 9, 11, 19–21, 23–37, 39–42
- LEP** Large Electron-Positron Collider. 11
- LHC** Large Hadron Collider. 11, 15, 25, 30, 40
- N2HDM** Next-to-Two-Higgs-Doublet Model. 1–5, 7, 11, 12, 19, 23, 31, 39
- NNLO** Next-to-next-to-leading order. 20, 31
- QCD** Quantum chromodynamics. 15, 20, 31
- SM** Standard Model of Particle Physics. 1–4, 7–10, 15, 20, 23–29, 31–33, 35, 36, 39, 40
- VBF** Higgs production via vector boson fusion. 15, 26, 27
- VEV** Vacuum expectation value. 4, 7–10, 12–14, 19, 20, 41–47, 49, 50
- VH** Vector-boson associated Higgs-boson production. 15
- WIMP** Weakly interacting massive particle. 1, 39

Bibliography

- [1] ATLAS collaboration, G. Aad et al., *Observation of a new particle in the search for the Standard Model Higgs boson with the ATLAS detector at the LHC*, *Phys. Lett.* **B716** (2012) 1–29, [1207.7214].
- [2] CMS collaboration, S. Chatrchyan et al., *Observation of a new boson at a mass of 125 GeV with the CMS experiment at the LHC*, *Phys. Lett.* **B716** (2012) 30–61, [1207.7235].
- [3] G. Bertone, D. Hooper and J. Silk, *Particle dark matter: Evidence, candidates and constraints*, *Phys. Rept.* **405** (2005) 279–390, [hep-ph/0404175].
- [4] PLANCK collaboration, P. A. R. Ade et al., *Planck 2015 results. XIII. Cosmological parameters*, *Astron. Astrophys.* **594** (2016) A13, [1502.01589].
- [5] PARTICLE DATA GROUP collaboration, C. Patrignani et al., *Review of Particle Physics*, *Chin. Phys.* **C40** (2016) 100001.
- [6] PLANCK collaboration, R. Adam et al., *Planck 2015 results. I. Overview of products and scientific results*, *Astron. Astrophys.* **594** (2016) A1, [1502.01582].
- [7] M. Bartelmann, *Neutrinos and structure formation in the universe*, in *Proceedings, fourth SFB-375 Ringberg workshop 'neutrino astrophysics' held Ringberg Castle, Tegernsee, Germany, 20-24 October 1997*, pp. 149–158, 1997, http://www.mpa-garching.mpg.de/SFB/ringberg_1997/bartelmann.ps.gz.
- [8] D. A. Ross and M. J. G. Veltman, *Neutral Currents in Neutrino Experiments*, *Nucl. Phys.* **B95** (1975) 135–147.
- [9] V. Silveira and A. Zee, *SCALAR PHANTOMS*, *Phys. Lett.* **161B** (1985) 136–140.
- [10] J. McDonald, *Gauge singlet scalars as cold dark matter*, *Phys. Rev.* **D50** (1994) 3637–3649, [hep-ph/0702143].
- [11] C. P. Burgess, M. Pospelov and T. ter Veldhuis, *The Minimal model of nonbaryonic dark matter: A Singlet scalar*, *Nucl. Phys.* **B619** (2001) 709–728, [hep-ph/0011335].
- [12] J. M. Cline, K. Kainulainen, P. Scott and C. Weniger, *Update on scalar singlet dark matter*, *Phys. Rev.* **D88** (2013) 055025, [1306.4710].
- [13] A. Beniwal, F. Rajec, C. Savage, P. Scott, C. Weniger, M. White et al., *Combined analysis of effective Higgs portal dark matter models*, *Phys. Rev.* **D93** (2016) 115016, [1512.06458].
- [14] A. Cuoco, B. Eiteneuer, J. Heisig and M. Krämer, *A global fit of the γ -ray galactic center excess within the scalar singlet Higgs portal model*, *JCAP* **1606** (2016) 050, [1603.08228].
- [15] GAMBIT collaboration, P. Athron et al., *Status of the scalar singlet dark matter model*, *Eur. Phys. J.* **C77** (2017) 568, [1705.07931].

- [16] N. G. Deshpande and E. Ma, *Pattern of Symmetry Breaking with Two Higgs Doublets*, *Phys. Rev.* **D18** (1978) 2574.
- [17] E. Ma, *Verifiable radiative seesaw mechanism of neutrino mass and dark matter*, *Phys. Rev.* **D73** (2006) 077301, [[hep-ph/0601225](#)].
- [18] R. Barbieri, L. J. Hall and V. S. Rychkov, *Improved naturalness with a heavy Higgs: An Alternative road to LHC physics*, *Phys. Rev.* **D74** (2006) 015007, [[hep-ph/0603188](#)].
- [19] L. Lopez Honorez, E. Nezri, J. F. Oliver and M. H. G. Tytgat, *The Inert Doublet Model: An Archetype for Dark Matter*, *JCAP* **0702** (2007) 028, [[hep-ph/0612275](#)].
- [20] C.-Y. Chen, M. Freid and M. Sher, *Next-to-minimal two Higgs doublet model*, *Phys. Rev.* **D89** (2014) 075009, [[1312.3949](#)].
- [21] A. Drozd, B. Grzadkowski, J. F. Gunion and Y. Jiang, *Extending two-Higgs-doublet models by a singlet scalar field - the Case for Dark Matter*, *JHEP* **11** (2014) 105, [[1408.2106](#)].
- [22] Y. Jiang, L. Li and R. Zheng, *Boosted scalar confronting 750 GeV di-photon excess*, [1605.01898](#).
- [23] M. Mühlleitner, M. O. P. Sampaio, R. Santos and J. Wittbrodt, *The N2HDM under Theoretical and Experimental Scrutiny*, *JHEP* **03** (2017) 094, [[1612.01309](#)].
- [24] T. D. Lee, *A Theory of Spontaneous T Violation*, *Phys. Rev.* **D8** (1973) 1226–1239.
- [25] J. F. Gunion, H. E. Haber, G. L. Kane and S. Dawson, *The Higgs Hunter's Guide*, *Front. Phys.* **80** (2000) 1–404.
- [26] G. C. Branco, P. M. Ferreira, L. Lavoura, M. N. Rebelo, M. Sher and J. P. Silva, *Theory and phenomenology of two-Higgs-doublet models*, *Phys. Rept.* **516** (2012) 1–102, [[1106.0034](#)].
- [27] M. Krawczyk, D. Sokółowska and B. Świeżewska, *2HDM with Z_2 symmetry in light of new LHC data*, *J. Phys. Conf. Ser.* **447** (2013) 012050, [[1303.7102](#)].
- [28] R. Coimbra, M. O. P. Sampaio and R. Santos, *ScannerS: Constraining the phase diagram of a complex scalar singlet at the LHC*, *Eur. Phys. J.* **C73** (2013) 2428, [[1301.2599](#)].
- [29] M. Aoki, S. Kanemura, K. Tsumura and K. Yagyu, *Models of Yukawa interaction in the two Higgs doublet model, and their collider phenomenology*, *Phys. Rev.* **D80** (2009) 015017, [[0902.4665](#)].
- [30] S. L. Glashow and S. Weinberg, *Natural conservation laws for neutral currents*, *Phys. Rev. D* **15** (Apr, 1977) 1958–1965.
- [31] G. D'Ambrosio, G. F. Giudice, G. Isidori and A. Strumia, *Minimal flavor violation: An Effective field theory approach*, *Nucl. Phys.* **B645** (2002) 155–187, [[hep-ph/0207036](#)].
- [32] R. S. Chivukula and H. Georgi, *Composite Technicolor Standard Model*, *Phys. Lett.* **B188** (1987) 99–104.
- [33] L. J. Hall and L. Randall, *Weak scale effective supersymmetry*, *Phys. Rev. Lett.* **65** (1990) 2939–2942.
- [34] A. J. Buras, P. Gambino, M. Gorbahn, S. Jager and L. Silvestrini, *Universal unitarity triangle and physics beyond the standard model*, *Phys. Lett.* **B500** (2001) 161–167, [[hep-ph/0007085](#)].

- [35] ATLAS, CMS collaboration, G. Aad et al., *Combined Measurement of the Higgs Boson Mass in pp Collisions at $\sqrt{s} = 7$ and 8 TeV with the ATLAS and CMS Experiments*, *Phys. Rev. Lett.* **114** (2015) 191803, [1503.07589].
- [36] P. Bechtle, O. Brein, S. Heinemeyer, O. Stål, T. Stefaniak, G. Weiglein et al., *HiggsBounds – 4: Improved Tests of Extended Higgs Sectors against Exclusion Bounds from LEP, the Tevatron and the LHC*, *Eur. Phys. J.* **C74** (2014) 2693, [1311.0055].
- [37] K. G. Klimenko, *Conditions for certain higgs potentials to be bounded below*, *Theoretical and Mathematical Physics* **62** (Jan, 1985) 58–65.
- [38] S. R. Coleman, *The Fate of the False Vacuum. 1. Semiclassical Theory*, *Phys. Rev.* **D15** (1977) 2929–2936.
- [39] C. G. Callan, Jr. and S. R. Coleman, *The Fate of the False Vacuum. 2. First Quantum Corrections*, *Phys. Rev.* **D16** (1977) 1762–1768.
- [40] J. Wittbrodt, *Phenomenological comparison of models with extended Higgs sectors*, Master’s thesis, KIT, Karlsruhe, 2016-09-29.
- [41] B. W. Lee, C. Quigg and H. B. Thacker, *Weak Interactions at Very High-Energies: The Role of the Higgs Boson Mass*, *Phys. Rev.* **D16** (1977) 1519.
- [42] ATLAS, CMS collaboration, G. Aad et al., *Measurements of the Higgs boson production and decay rates and constraints on its couplings from a combined ATLAS and CMS analysis of the LHC pp collision data at $\sqrt{s} = 7$ and 8 TeV*, *JHEP* **08** (2016) 045, [1606.02266].
- [43] M. E. Peskin and T. Takeuchi, *Estimation of oblique electroweak corrections*, *Phys. Rev.* **D46** (1992) 381–409.
- [44] W. Grimus, L. Lavoura, O. M. Ogreid and P. Osland, *A Precision constraint on multi-Higgs-doublet models*, *J. Phys.* **G35** (2008) 075001, [0711.4022].
- [45] W. Grimus, L. Lavoura, O. M. Ogreid and P. Osland, *The Oblique parameters in multi-Higgs-doublet models*, *Nucl. Phys.* **B801** (2008) 81–96, [0802.4353].
- [46] GFITTER GROUP collaboration, M. Baak, J. Cúth, J. Haller, A. Hoecker, R. Kogler, K. Mönig et al., *The global electroweak fit at NNLO and prospects for the LHC and ILC*, *Eur. Phys. J.* **C74** (2014) 3046, [1407.3792].
- [47] F. Mahmoudi and O. Stal, *Flavor constraints on the two-Higgs-doublet model with general Yukawa couplings*, *Phys. Rev.* **D81** (2010) 035016, [0907.1791].
- [48] T. G. Collaboration, *Talk at eps 2016*, .
- [49] H. E. Haber and H. E. Logan, *Radiative corrections to the $Z b$ anti- b vertex and constraints on extended Higgs sectors*, *Phys. Rev.* **D62** (2000) 015011, [hep-ph/9909335].
- [50] XENON collaboration, E. Aprile et al., *First Dark Matter Search Results from the XENON1T Experiment*, *Phys. Rev. Lett.* **119** (2017) 181301, [1705.06655].
- [51] G. Belanger, F. Boudjema, A. Pukhov and A. Semenov, *MicrOMEGAs: A Program for calculating the relic density in the MSSM*, *Comput. Phys. Commun.* **149** (2002) 103–120, [hep-ph/0112278].
- [52] G. Belanger, F. Boudjema, A. Pukhov and A. Semenov, *MicrOMEGAs 2.0: A Program to calculate the relic density of dark matter in a generic model*, *Comput. Phys. Commun.* **176** (2007) 367–382, [hep-ph/0607059].

- [53] D. Barducci, G. Belanger, J. Bernon, F. Boudjema, J. Da Silva, S. Kraml et al., *Collider limits on new physics within micrOMEGAs 4.3*, *Comput. Phys. Commun.* **222** (2018) 327–338, [1606.03834].
- [54] W. H. Press, S. A. Teukolsky, W. T. Vetterling and B. P. Flannery, *Numerical Recipes in C (2Nd Ed.): The Art of Scientific Computing*. Cambridge University Press, New York, NY, USA, 1992.
- [55] A. Belyaev, N. D. Christensen and A. Pukhov, *CalcHEP 3.4 for collider physics within and beyond the Standard Model*, *Comput. Phys. Commun.* **184** (2013) 1729–1769, [1207.6082].
- [56] F. Staub, *SARAH 4 : A tool for (not only SUSY) model builders*, *Comput. Phys. Commun.* **185** (2014) 1773–1790, [1309.7223].
- [57] R. V. Harlander, S. Liebler and H. Mantler, *SusHi Bento: Beyond NNLO and the heavy-top limit*, *Comput. Phys. Commun.* **212** (2017) 239–257, [1605.03190].
- [58] A. Djouadi, J. Kalinowski and M. Spira, *HDECAY: A Program for Higgs boson decays in the standard model and its supersymmetric extension*, *Comput. Phys. Commun.* **108** (1998) 56–74, [hep-ph/9704448].
- [59] J. M. Butterworth et al., *THE TOOLS AND MONTE CARLO WORKING GROUP Summary Report from the Les Houches 2009 Workshop on TeV Colliders*, in *Physics at TeV colliders. Proceedings, 6th Workshop, dedicated to Thomas Binoth, Les Houches, France, June 8-26, 2009*, 2010, 1003.1643.
- [60] A. Djouadi, J. Kalinowski, M. Muehlleitner and M. Spira, *HDECAY: Twenty++ Years After*, 1801.09506.
- [61] CMS collaboration, C. Collaboration, *Update of the search for the Standard Model Higgs boson decaying into WW in the vector boson fusion production channel*, .
- [62] E. M. Dolle and S. Su, *The Inert Dark Matter*, *Phys. Rev.* **D80** (2009) 055012, [0906.1609].